Why Do Modeled and Observed Surface Wind Stress Climatologies Differ in the Trade Wind Regions?

ISLA R. SIMPSON AND JULIO T. BACMEISTER

Climate and Global Dynamics Laboratory, National Center for Atmospheric Research, Boulder, Colorado

IRINA SANDU AND MARK J. RODWELL

European Centre for Medium-Range Weather Forecasts, Reading, United Kingdom

(Manuscript received 18 April 2017, in final form 17 August 2017)

ABSTRACT

Global climate models (GCMs) exhibit stronger mean easterly zonal surface wind stress and near-surface winds in the Northern Hemisphere (NH) trade winds than observationally constrained reanalyses or other observational products. A comparison, between models and reanalyses, of the processes that contribute to the zonal-mean, vertically integrated balance of momentum reveals that this wind stress discrepancy cannot be explained by either the resolved dynamics or parameterized tendencies that are common to each. Rather, a substantial residual exists in the time-mean momentum balance of the reanalyses, pointing toward a role for the analysis increments. Indeed, they are found to systematically weaken the NH near-surface easterlies in winter, thereby reducing the diagnosed surface wind stress. Similar effects are found in the Southern Hemisphere, and further analysis of the spatial structure and seasonality of these increments demonstrates that they act to weaken the near-surface flow over much of the low-latitude oceans in both summer and winter. This suggests an erroneous/missing process in GCMs that constitutes a missing drag on the low-level zonal flow over oceans. This indicates either a misrepresentation of the drag between the surface and the atmosphere or a missing internal atmospheric process that amounts to an additional drag on the low-level zonal flow. If the former is true, then observation-based surface stress products, which rely on similar drag formulations to GCMs, may be underestimating the strength of the easterly surface wind stress.

1. Introduction

Since the early days of global climate modeling and numerical weather prediction, models have increased substantially in resolution and complexity, pushing toward an ever more realistic representation of Earth's atmosphere and climate. There are, however, certain processes within the atmosphere that still cannot be resolved with global models and are unlikely to be in the near future, and so we must continue to rely on subgrid-scale parameterizations to represent them. A continuing necessity, therefore, is to ensure that these parameterizations are faithfully representing the processes for which they are intended. This is made all the more challenging by the fact that many of these processes cannot be extensively observed on a global scale.

One aspect that global climate models (GCMs) should simulate with fidelity is the climatological characteristics of the large-scale atmospheric circulation, including the overall balances of momentum. This study is concerned with the representation of processes that contribute to this overall balance of momentum within the atmosphere in GCMs. The climatological momentum balance that a GCM achieves will depend on the behavior of the resolved large-scale flow, the subgrid-scale parameterizations, and the interaction between them. A number of parameterizations play a key role in the momentum balance of a GCM. First and foremost is the vertical transfer of momentum between the atmosphere and the solid earth and ocean achieved through surface drag and subgrid-scale turbulent effects. Many models also now include a representation of the nonlinear blocking (Lott and Miller 1997) and turbulent form drag (Beljaars et al. 2004) effects of subgrid-scale orography, and, since the 1980s, orographic gravity wave drag schemes have been implemented in most GCMs to mimic the transfer of momentum into the upper atmosphere by orographically generated gravity waves

Corresponding author: Isla R. Simpson, islas@ucar.edu

DOI: 10.1175/JCLI-D-17-0255.1

(Palmer et al. 1986; McFarlane 1987). Aside from momentum transfers between the surface and the atmosphere, many models also include parameterized representations of the vertical transfer of momentum within the atmosphere itself, by convection (Zhang and Cho 1991) and the gravity waves that it generates (Richter et al. 2010).

The circulation climatology produced by a GCM will depend on the mutual interaction between these various components. How to configure these parameterizations to reach a climate that is representative of the real world is not a solved problem, by any means. This is readily apparent from the fact that models vary widely in the relative partitioning of the overall surface drag over land into boundary layer and subgrid-scale orography components (Zadra 2015; Sandu et al. 2016) and the overall stratospheric wave driving into resolved flow and parameterized components (Butchart et al. 2011). To simulate the atmosphere with fidelity, not only must the theoretical principles on which the parameterizations are built be correct, but the parameters that govern the behavior of these schemes must be observationally constrained, and, for many aspects, an adequate observational constraint is lacking.

The impact of changes to the configuration of a particular parameterization can be substantial. For example, recent studies have shown that varying the contribution of turbulent orographic form drag and orographic blocking can have a significant impact on the large-scale circulation, both in numerical weather prediction and climate modeling contexts (Sandu et al. 2016; Pithan et al. 2016; van Neikerk et al. 2017). Garfinkel et al. (2011) also found that varying the parameters that govern surface drag over the oceans impacted the Southern Hemisphere (SH) circulation and, in reduced-complexity models, varying the surface drag strength was shown to result in a change in the location of the midlatitude westerlies (Chen et al. 2007; Polichtchouk and Shepherd 2016). In many of these studies, the parameter range explored has been within a realistic uncertainty range, but given that these uncertainties are large, so too is the impact on the modeled circulation. It is therefore possible that improvements to the subgrid parameterizations could lead to an improved representation of the large-scale climate, but also that a reasonable large-scale climate could be obtained for the wrong reasons, through the use of tuning parameters that are not well constrained by observations.

When it comes to assessing the fidelity of model parameterizations, there is much to be gained by exploiting aspects of the atmosphere that are better constrained at present, such as the large-scale circulation. Consideration of the large-scale balances that exist when a model's flow is constrained to follow that of the real world, as is the case in data assimilation (i.e., analyses and reanalysis) or nudging procedures, can lead to identification of the tendencies that must be provided by the subgrid-scale parameterizations. For example, Trenberth (1997) used such an approach to infer surface heat and moisture fluxes as a residual from the climatological thermodynamic and moisture balances. Another complementary approach is to assess the short-term drifts of model forecasts away from the real-world evolution or, equivalently, the incremental adjustments that are required to continuously constrain a model to follow that real-world evolution. Examples of this approach include Wallace et al. (1983), who demonstrated the need for an envelope orography through 1-day model forecast errors; Klinker and Sardeshmukh (1992), who used initial tendency errors to identify issues with certain parameterizations in one forecast model; Rodwell and Palmer (2007), who used initial tendency errors to evaluate different climate model configurations; and McLandress et al. (2012) and Pulido (2014), who used analysis increments to infer missing stratospheric gravity wave drag. The principle behind each of these studies is that constraining the large-scale circulation to that of the real world eliminates any errors that could arise through slow atmospheric adjustments to nonlocal processes and allows for identification of those that arise through local, faster, parameterized processes, allowing one to home in on the problem.

The issue to be addressed here is the rather systematic difference in zonal surface wind stress between free-running GCMs [those that participated in phase 5 of the Coupled Model Intercomparison Project (CMIP5)] and observation-based products in the Northern Hemisphere (NH) low latitudes during winter [noted in Simpson et al. (2014, hereafter S14) and shown here in Fig. 1]. The majority of GCMs exhibit stronger surface wind stress in the easterly trades region than observation-based products. To gain some understanding of the reason behind this discrepancy, we first compare the climatological vertically integrated momentum balance in the CMIP5 models with that in observationally constrained reanalyses. It is demonstrated that this surface wind stress difference cannot be explained by a difference in the momentum transfer terms that are common to both. Rather, in the reanalyses, a momentum imbalance exists, with the analysis increments making a systematic contribution by weakening the strength of the low-level flow. In the spirit of the above studies, we then use these analysis

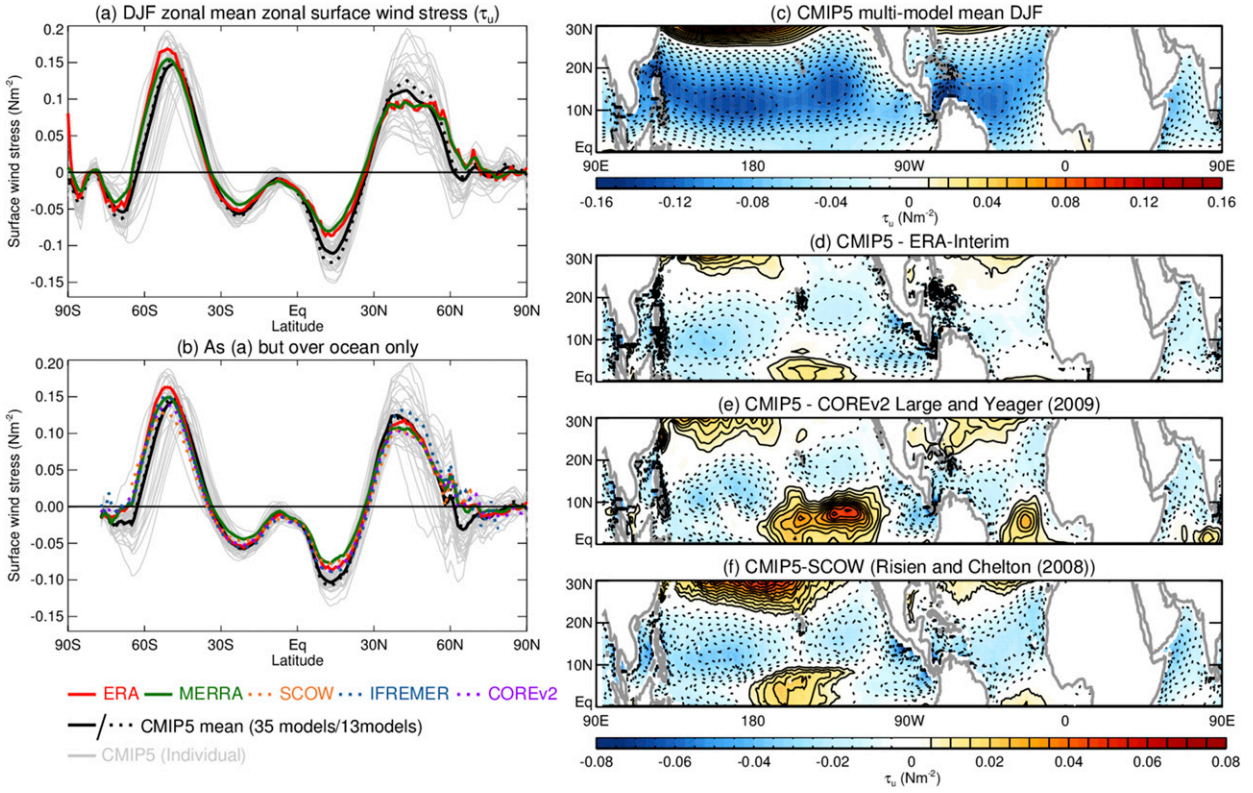

FIG. 1. (a) Zonal-mean DJF climatologies of τ_u. (b) As in (a), but for the zonal mean over ocean grid points only; shown are ERA-Interim (red), MERRA (green), each individual CMIP5 model (gray), the multimodel mean of all 35 CMIP5 models (black solid), and the multimodel mean of the 13-model subset of CMIP5 used in the momentum balance analysis (black dotted). Also shown are the COREv2 dataset (purple dotted; Large and Yeager 2009), the SCOW dataset (orange dotted; Risien and Chelton 2008), and the IFREMER dataset (blue dotted; Bentamy et al. 2013) (note that these data only exist over the ocean). (c) The CMIP5 multimodel mean (35 models) DJF climatology of τ_u in the NH low latitudes. The difference between the CMIP5 multimodel mean τ_u and (d) ERA-Interim over oceans, (e) COREv2, and (f) SCOW.

increments to infer an erroneous, or inadequate, representation of drag on the low-level flow, over oceans, in the models that underlie the reanalyses. Given that these underlying models are based on similar physics to those in CMIP5, this error is likely also present in the CMIP5 models, contributing to biases in their near-surface wind. While the NH low latitudes during winter will be our primary focus, this same issue is present in other regions and seasons.

Section 2 describes the momentum balance diagnostic that will be used along with some basic background on the formulation of ocean surface drag parameterizations. Section 3 then describes the model simulations and observation-based products that will be used. The vertically integrated momentum balance results are discussed in section 4, and the details of the role of the analysis increments are presented in section 5. Further analysis on spatial and seasonal variations is provided in section 6, and concluding discussions are given in section 7.

2. Basic theory and diagnostics

a. The vertically integrated momentum balance

GCMs obey the following equation for the time evolution of zonal wind on a pressure surface:

$$\frac{\partial u}{\partial t} = fv - \frac{1}{a\cos\phi}\frac{\partial \Phi}{\partial \lambda} - \frac{1}{a\cos^2\phi}\frac{\partial (uv\cos^2\phi)}{\partial \phi} - \frac{1}{a\cos\phi}\frac{\partial (uu)}{\partial \lambda} - \frac{\partial (u\omega)}{\partial p} + F_u + X, \quad (1)$$

where u is zonal wind, v is meridional wind, ω is vertical (pressure) velocity, f is the Coriolis parameter, Φ is geopotential, and λ, ϕ, and p are longitude, latitude, and pressure, respectively (Andrews et al. 1987). The last two terms represent the zonal tendencies associated with parameterized processes, where F_u refers to the tendencies due to momentum transport by turbulent eddies, surface drag, and turbulent orographic form drag (or form drag due to small-scale topography), and X

denotes the tendencies from any other parameterized processes that a model may have, such as orographic blocking, orographic and nonorographic gravity wave drag, convective momentum transport, or horizontal diffusion. Calculating the mass-weighted vertical integral of (1) according to

$$|\cdot| = \frac{1}{g}\int_0^{p_s} (\cdot)\, dp, \tag{2}$$

where p_s is the surface pressure and g is the acceleration due to gravity, yields the following:

$$\left|\frac{\partial u}{\partial t}\right| = f|v| - \left|\frac{1}{a\cos\phi}\frac{\partial \Phi}{\partial \lambda}\right| - \left|\frac{1}{a\cos^2\phi}\frac{\partial (uv\cos^2\phi)}{\partial \phi}\right| - \left|\frac{1}{a\cos\phi}\frac{\partial (uu)}{\partial \lambda}\right| - u_s\omega_s - \tau_u + |X|, \tag{3}$$

where the term involving ω has reduced to a term involving only the surface winds u_s and ω_s, and the vertical integral of F_u has become $-\tau_u$, where τ_u is the downward zonal surface wind stress (i.e., the zonal stress the atmosphere exerts on the surface, with the exception of the contribution from orographic gravity wave drag and blocking).[1]

This balance can be simplified further by taking the zonal mean. Denoting the zonal average as $\overline{(\cdot)}$ and the zonal average of the second term on the right-hand side (RHS) of (3) as the mountain torque M, with some rearranging, the overall vertically integrated and zonally averaged momentum balance can be written as

$$\overline{\tau_u} = f|\overline{v}| + M - \overline{\left|\frac{1}{a\cos^2\phi}\frac{\partial (uv\cos^2\phi)}{\partial \phi}\right|} - \overline{\left|\frac{1}{a\cos\phi}\frac{\partial (uu)}{\partial \lambda}\right|} - \overline{u_s\omega_s} - \left|\frac{\partial \overline{u}}{\partial t}\right| + |\overline{X}|. \tag{4}$$

That is, the zonal-mean surface wind stress at the lower boundary must be balancing the vertically integrated sum of all the terms on the RHS. These include the advective tendencies by the large-scale flow, the mountain torque, and other parameterized tendencies in the free atmosphere, which in practice is dominated by orographic gravity wave drag and blocking in this vertical integral. The first and fourth terms on the RHS of (4) are not exactly zero in this formulation due to contributions from pressure levels that intersect topography. The fifth term is also not exactly zero owing to the contribution from nonzero pressure vertical velocities along the sloping surface. The fourth and fifth terms, while included, can essentially be neglected.

b. *The formulation of surface drag parameterizations over oceans*

The zonal surface stress $\overline{\tau}_u$ in (4) consists of contributions from boundary layer turbulence over both land and ocean as well as stresses from subgrid-scale orographic form drag schemes. Since a component of the discussion that follows will center around the representation of surface drag between the atmosphere and ocean, we give a brief overview of the methods used to represent this process in models. A bulk formulation is typically used to describe the exchange of momentum between the ocean surface and the atmosphere in terms of large-scale properties on the lowest model level. The vector surface downward wind stress, which consists of u and v components, is given by

$$\boldsymbol{\tau}_{\mathbf{v}} = \rho_s C_D |\mathbf{v}_s| \mathbf{v}_s, \tag{5}$$

where ρ_s is the surface air density, $\mathbf{v}_s$ is the vector wind on the lowest model level, and $|\mathbf{v}_s|$ here refers to its magnitude. The drag coefficient C_D is a function of stability and the surface roughness, which itself depends on the wind speed. An appropriate value of C_D must be determined to yield an appropriate exchange of momentum between the ocean and atmosphere for a given wind speed and atmospheric stability. In practice, the estimates of C_D are based on empirical functions that describe the drag coefficient in neutrally stable conditions C_{DN} as a function of wind speed at a reference height (typically 10 m from the surface). These empirical functions have been determined through flux tower observations of the vertical momentum flux at various oceanic sites (Large and Pond 1982; Yelland et al. 1998; Edson et al. 2013). Given these values of C_{DN}, one has to then determine the value of C_D given the wind speeds at the height of the lowest model level and the atmospheric stability. This is achieved through Monin–Obhukov similarity theory, which determines the vertical variation of the flow and the turbulent fluxes under the given turbulent conditions.

Many formulations of C_{DN} as a function of 10-m neutral wind speed exist (Large and Pond 1982; Smith 1988; Trenberth et al. 1989; Large et al. 1994; Fairall et al. 1996). These are based on information from a limited number of measurements, owing to the

[1] The term τ_u excludes the orographic gravity wave drag component due to data availability. While a more natural decomposition might be to include the orographic blocking and orographic gravity wave drag in F_u, which would leave $-\tau_u$ as the true total zonal stress the surface exerts on the atmosphere, the surface stress output for the CMIP5 models does not include the orographic gravity wave drag contribution and so we combine that with the other parameterized tendencies that we do not have in X.

TABLE 1. List of historical CMIP5 simulations used in the momentum balance calculation.

Model	Expansion
BCC_CSM1.1	Beijing Climate Center, Climate System Model, version 1.1
BCC_CSM1.1(m)	Beijing Climate Center, Climate System Model, version 1.1, moderate resolution
CanESM2	Second Generation Canadian Earth System Model
CCSM4	Community Climate System Model, version 4
GFDL CM3	Geophysical Fluid Dynamics Laboratory Climate Model, version 3
GFDL-ESM2G	Geophysical Fluid Dynamics Laboratory Earth System Model with Generalized Ocean Layer Dynamics (GOLD) component
GFDL-ESM2M	Geophysical Fluid Dynamics Laboratory Earth System Model with Modular Ocean Model 4 (MOM4) component
IPSL-CM5A-MR	L'Institut Pierre-Simon Laplace Coupled Model, version 4, coupled with NEMO, mid resolution
MIROC5	Model for Interdisciplinary Research on Climate, version 5
MIROC-ESM	Model for Interdisciplinary Research on Climate, Earth System Model
MIROC-ESM-CHEM	Model for Interdisciplinary Research on Climate, Earth System Model, Chemistry Coupled
MRI-CGCM3	Meteorological Research Institute Coupled Atmosphere–Ocean General Circulation Model, version 3
NorESM1-M	Norwegian Earth System Model, version 1 (intermediate resolution)

challenges of measuring momentum fluxes over the open oceans, and they continue to undergo revisions as additional observational information becomes available (Fairall et al. 2003; Edson et al. 2013). The appropriate values of C_{DN} are still somewhat uncertain, particularly at the lowest and highest wind speeds, as can be seen in the recent observational analysis of Edson et al. (2013, their Fig. 6).

3. Model simulations and observational products

a. The CMIP5 simulations

We make use of the CMIP5 coupled historical simulations from 1979 to 2005. The initial motivating analysis of surface wind stress differences between these models and observational products (Fig. 1) makes use of all available ensemble members for 35 different CMIP5 models. The models and members used are the same as listed in Table 1 of S14. The vertically integrated momentum balance calculation requires 6-hourly instantaneous fields on a high vertical resolution, and so this analysis is restricted to a subset of 13 models and one ensemble member for each, also as in S14, and listed here in Table 1. These models are quite representative of CMIP5 as a whole and were chosen based on the fact that they have the necessary data to obtain a reasonable closure of the momentum balance (see S14 for more details). The vertically integrated momentum balance calculation [(4)] follows the procedure outlined in detail in S14 and summarized only briefly here. Each term is calculated on the 17 standard CMIP5 pressure levels (i.e., 1000, 925, 850, 700, 600, 500, 400, 300, 250, 200, 150, 100, 70, 50, 30, 20, and 10 hPa) before vertically integrating, and this vertical integral is performed on a monthly mean basis with the monthly mean surface pressure at the lower boundary. While this may introduce some error, compared to vertically integrating on an instantaneous basis (Trenberth et al. 1993), it is the best that can be done with the available data, and, as will be shown, the balance calculated in this way does close sufficiently well. The horizontal momentum flux terms in (4) were evaluated using 6-hourly instantaneous u and v, which were obtained through vertical interpolation of the 6-hourly model level data onto the 17 standard pressure levels. Unfortunately, the additional parameterized tendencies X are not available for these models, and so this term must be omitted from the balance.

For plotting purposes, owing to small-scale noise that appears in the mountain torque, all terms were isotropically smoothed in the spectral domain according to Sardeshmukh and Hoskins [1984, their Eq. (9), with coefficients $n_0 = 21$ and $r = 1$]. When τ_u is shown alongside the budget terms, it is similarly smoothed, but when it is shown alone, no smoothing is applied.

b. The reanalysis products

The primary reanalysis product used in the following is ERA-Interim (Dee et al. 2011). ERA-Interim is produced using a four-dimensional variational data assimilation system with a 12-h analysis cycle, as depicted schematically in Fig. 2a (see also Rodwell and Palmer 2007). The analysis state represents the most plausible state of the atmosphere given the observations and forecast projection combined. In essence, at a given time t, a 12-h forecast is performed, initialized from the analysis state. The observational information available over the following 12-h period is then combined with this forecast model projection to reach the analysis state at time $t + 12$. We refer to the state produced by the initialized forecast alone as the *forecast state* and the difference between the analysis state and the forecast

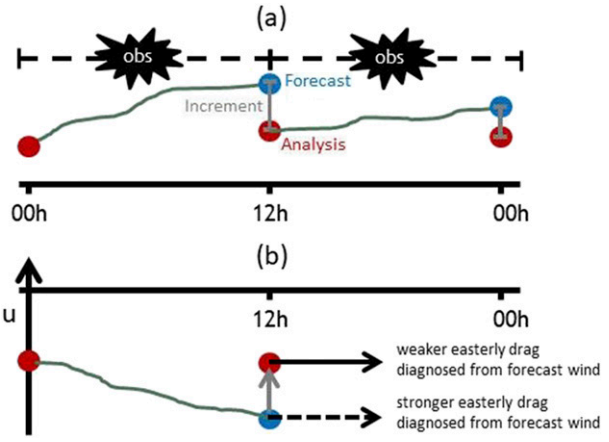

FIG. 2. (a) Schematic depiction of the reanalysis procedure. Forecasts (green lines) are initialized from the analysis state (red circles) at time t. This produces the forecast state at time $t + 12$ (blue circles). Information from the model forecast and observations over the 12-h interval are combined to produce the analysis state at time $t + 12$. The analysis increment is calculated as the difference between the forecast and the analysis state at each 0- and 12-h time each day. (b) Schematic depiction of the influence that a reduction in low-level easterly flow by the analysis increments would have on the surface drag of the subsequent 12-h forecast, as discussed in section 5a.

state (i.e., the impact of the assimilated observations) as the *analysis increment*. ERA-Interim assimilates a myriad of observations (Dee et al. 2011), but of particular relevance for the following diagnosis is that it assimilates near-surface wind measurements from ships and buoys along with scatterometer winds after 1992.

The momentum balance calculation is performed for ERA-Interim using the same methodology as outlined above for CMIP5; that is, the same 17 pressure levels are used, and the vertical integral is performed on a monthly mean basis. While this may not be the most accurate calculation that could be performed, given the greater data availability in ERA-Interim, our goal is to compute the balance in as similar a way as possible to that of the CMIP5 models, to allow for a like-with-like comparison. The u, v, ω, Φ, and p_s used in the calculation are those of the analysis state (red circles in Fig. 2a), whereas, since τ_u is a model-derived quantity, it is averaged over each 12-h forecast (green lines in Fig. 2a).

A companion analysis with MERRA (Rienecker et al. 2011) is presented in appendix A and lends support to the main conclusions drawn from ERA-Interim. MERRA climatologies of τ_u are also shown in the main body of the text for comparison. Rather than using the direct τ_u output from MERRA, we show the vertical integral of the zonal wind tendencies due to turbulence (DUDTTRB) since, unlike ERA-Interim, the former does not contain the stress from the subgrid-scale orographic form drag scheme. This detail is, however, unimportant in the low latitudes where the direct τ_u output and that derived from the turbulence tendencies are very comparable.

TABLE 2. Summary of observation-based datasets and time periods used. These datasets are described in more detail in appendix B.

Dataset	τ_u	u_{10}	u_{10N}
COREv2 (Large and Yeager 2009)	1979–2005	—	—
SCOW (Risien and Chelton 2008)	1999–2007	—	1999–2007
IFREMER (Bentamy et al. 2013)	1999–2009	—	1999–2009
WASWind (Tokinaga and Xie 2011)	—	1979–2005	—

c. *Observation-based products of surface wind stress and near-surface wind*

We will also compare the reanalysis surface wind stress and 10-m zonal winds with four other products that are more directly derived from in situ or satellite-based measurements: CORE version 2 (COREv2; Large and Yeager 2009), Scatterometer Climatology of Ocean Winds (SCOW; Risien and Chelton 2008), Institut Français de Recherche pour L'Exploitation de la Mer (IFREMER; Bentamy et al. 2013), and Wave- and Anemometer-Based Sea Surface Wind (WASWind; Tokinaga and Xie 2011). These datasets, summarized in Table 2 and described in more detail in appendix B, mostly make use of in situ 10-m wind measurements from ships and buoys or satellite-based scatterometer measurements.

Scatterometer measurements have the advantage over in situ measurements in that they provide a much more global coverage. They measure backscattered radiation that is altered by the presence of wind stress–generated capillary waves on the ocean surface. The quantity that scatterometers are measuring is, therefore, most closely related to stress. However, given the difficulty in actually measuring stress over the ocean, in situ stress measurements are too sparse to be used for calibration, and scatterometer measurements are actually calibrated against equivalent neutral 10-m winds from buoys or radiometers. An empirically derived geophysical model function (GMF) relates the backscattered radiation to wind speed and direction, and this GMF is derived through matching the back scattered radiation with true observed wind speeds and directions that have been adjusted to neutral conditions and 10-m height (e.g., Wentz and Smith 1999). Therefore, the product that is actually retrieved from the scatterometer

measurements is the 10-m vector wind, adjusted to neutral conditions $\mathbf{v}_{10N}$. The stress vector can then be readily derived from this using $\boldsymbol{\tau}_{\mathbf{v}} = \rho_s C_{DN} |\mathbf{v}_{10N}| \mathbf{v}_{10N}$, but this means that scatterometer wind stress estimates are not free from the errors that may be present in the functional form of C_{DN}. Indeed, Risien and Chelton (2008) demonstrated that the stress estimates obtained from the Quick Scatterometer (QuikSCAT) can differ depending on which formulation of C_{DN} is used.

4. Comparisons of τ_u and the vertically integrated momentum balance

a. τ_u in CMIP5 vs observational products

The initial motivation for this analysis is the systematic difference in zonal-mean τ_u between the CMIP5 models and the reanalyses in the NH low latitudes during December–February (DJF). Figure 1a demonstrates that almost all models exhibit a zonal-mean easterly surface wind stress that is stronger than that in either ERA-Interim or MERRA, with the multimodel mean having roughly 20% more easterly stress in comparison to the reanalyses at around 15°N. A similar difference was noted in the annual mean by Lee et al. (2013). To compare with the other observation-based products, which are available only over the oceans, Fig. 1b shows the zonal-mean τ_u over ocean grid points only. The fact that the models exhibit more easterly τ_u than the reanalyses is also apparent when one considers only the ocean grid points, and, here, the other observation-based products compare well with the reanalyses.

The spatial structure of the zonal surface wind stress over oceans in the NH low latitudes for the CMIP5 multimodel mean and the difference between the CMIP5 multimodel mean and ERA-Interim, COREv2, and SCOW (Figs. 1c–f) make clear that across the whole of the NH low-latitude oceans, between around 10° and 20°N, the CMIP5 τ_u is more easterly than any of the observation-based products.

b. The vertically integrated momentum balance

With an aim to shed light on the reasons behind this τ_u discrepancy, following on from preliminary analysis (see the appendix of S14), we now compare the vertically integrated momentum balance between the 13-model subset of CMIP5 and ERA-Interim in detail. The 13-model subset compares well with the 35 models in terms of its τ_u mean climatology (Figs. 1a,b). The momentum balance analysis is performed for each month of the year, and we focus on the low latitudes between 30°S and 30°N (Fig. 3).

Figures 3a, 3d, and 3g again demonstrate the stronger easterly τ_u in CMIP5, but here, the τ_u difference is actually apparent throughout much of the year in the NH, with the difference structure following the seasonal evolution of τ_u itself, exhibiting a maximum in winter when the easterly trade winds are the strongest. There is also a hint of a similar difference in the SH, maximizing in the SH winter, although it is of smaller magnitude. We will return to the SH in section 6.

The vertically integrated sum of terms on the RHS of (4) (Figs. 3b,e,h), which should balance τ_u, can be used to gain some insights into the reasons behind the τ_u difference. Recall that the parameterized tendencies X are excluded here since these are not available for CMIP5, and so we refer to the RHS of (4) as the resolved dynamics terms since it is composed of terms that solely involve the large-scale resolved circulation. Focusing first on the CMIP5 balance, a comparison of Figs. 3a and 3b demonstrates that the balance of terms in (4) is achieved rather well, despite the omission of X. The residual between the resolved dynamics terms and τ_u is small in the NH low latitudes (Fig. 3c), but it becomes larger toward the north where orographic drag in X becomes important. It is also unclear whether all the CMIP5 models include the stresses from subgrid-scale orographic schemes in their surface wind stress output, and so this may also contribute to some discrepancies there as well. Therefore, for now we focus our analysis on the NH low latitudes, even though there are differences in τ_u in the midlatitudes too (Fig. 1a).

For the NH low latitudes, the question is, can we explain the difference in τ_u between CMIP5 and ERA-Interim (Fig. 3a vs Fig. 3d) through a difference in the resolved dynamics terms? If so, that would imply that τ_u differs because the vertically integrated momentum transports by the large-scale circulation differ. However, this is not the case. The sum of the resolved dynamics terms in both the CMIP5 models and ERA-Interim (Figs. 3b,e,h) are actually rather similar in the NH low latitudes. The sum of the resolved dynamics terms in ERA-Interim is slightly less easterly than CMIP5, but not to the degree that can explain the τ_u difference (cf. Figs. 3g and 3h).

The vertically integrated resolved dynamics terms and τ_u do not balance in ERA-Interim to the same degree that they do in the free-running models, leaving a residual that is on the order of 20%–30% of the τ_u climatology. While this residual is reduced slightly with the inclusion of the other parameterized tendencies X (see Fig. 3i), the majority remains, and a large component of the τ_u difference between CMIP5 and ERA-Interim reflects this residual in the ERA-Interim balance as opposed to a difference in the resolved or parameterized tendencies.

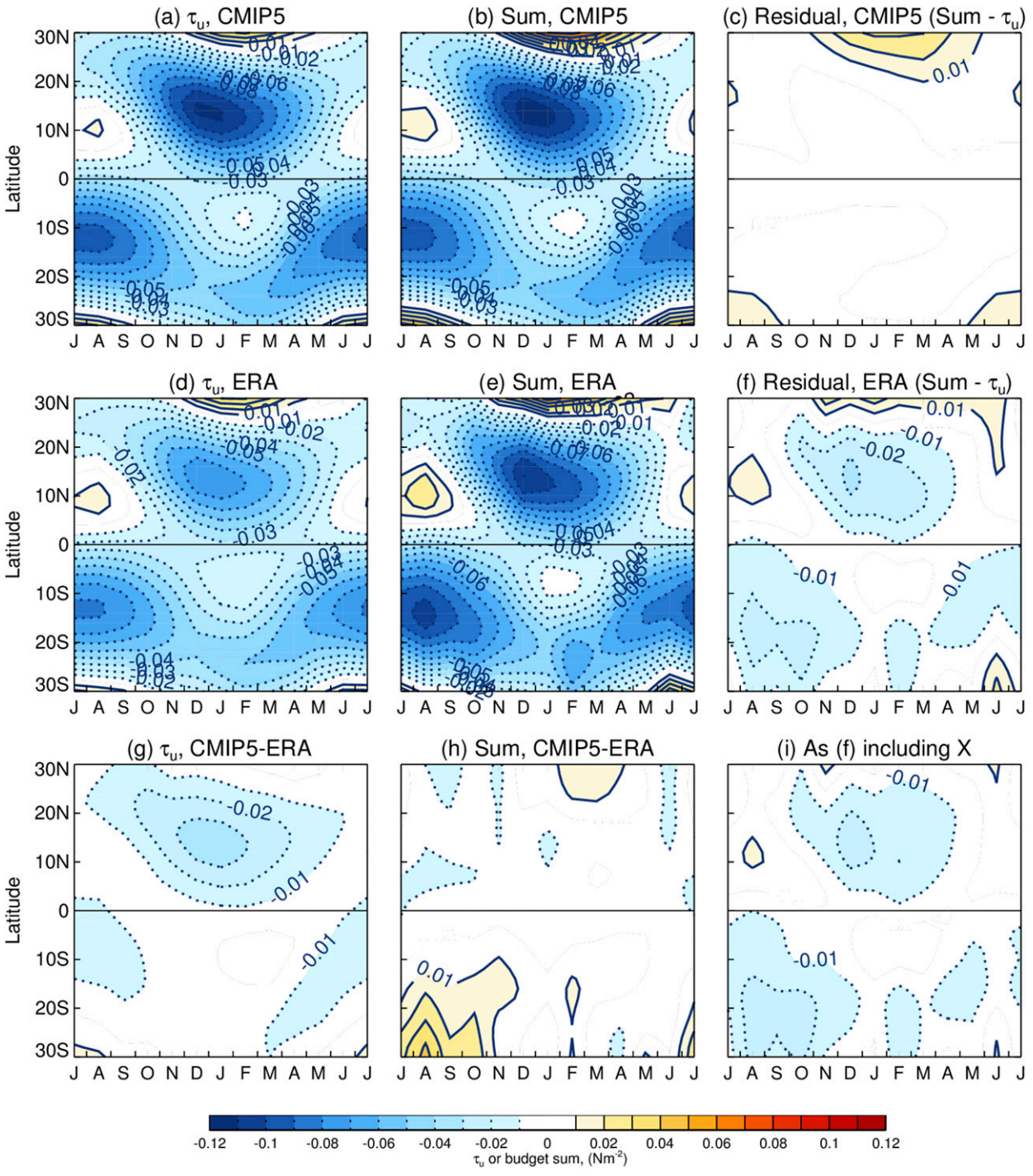

FIG. 3. Vertically integrated momentum balance in the low latitudes (from 30°S to 30°N) as a function of season. The budget for the mean of the 13 CMIP5 models: (a) the surface wind stress, (b) the resolved dynamics terms [i.e., the terms on the RHS of (4)], and (c) the difference between them. (d)–(f) As in (a)–(c), but for ERA-Interim. The difference between CMIP5 and ERA-Interim (g) τ_u and (h) the resolved dynamics terms. (i) The ERA-Interim budget residual obtained when including all additional parameterized tendencies X.

To put this another way, the weaker surface wind stress in ERA-Interim compared to CMIP5 cannot be fully explained by a difference in either the resolved dynamics terms or parameterized tendencies that are present in the vertically integrated momentum balance. If the ERA-Interim surface wind stress were instead calculated as a residual (i.e., what is required to balance the vertically integrated tendencies throughout the

atmosphere above), this would amount to a larger wind stress, more in line with that in CMIP5. Quantitatively, the DJF-averaged zonal-mean τ_u at 14°N for the CMIP5 mean is $-0.107\,\mathrm{N\,m^{-2}}$ and that for ERA-Interim is $-0.074\,\mathrm{N\,m^{-2}}$. In contrast, the ERA-Interim stress calculated as a residual is $-0.095\,\mathrm{N\,m^{-2}}$ (i.e., closer to CMIP5). Similar conclusions can be drawn for MERRA (see appendix A). This imbalance suggests that the analysis increments are leading to the weaker τ_u in the reanalysis.

5. The influence of the analysis increments during DJF

a. *The contribution of the analysis increments to the ERA-Interim zonal-mean climatology*

The momentum imbalance that exists in ERA-Interim, discussed above, may be associated with the analysis increments. Recall that the ERA-Interim momentum balance was computed using the meteorological fields of the analysis state (i.e., the closest estimate to the real-world state), but the surface wind stress was averaged over the 12-h forecast. If the underlying forecast model and assimilated observations were perfect, then there would be no analysis increments, and the momentum balance calculated in this way should close just as well for ERA-Interim as it does for the free-running CMIP5 models. Instead, the analysis increments play a role, upsetting this balance.

Systematic analysis increments occur in our region of interest (Fig. 4b). In particular, they act to reduce the easterly flow in the NH low latitudes where the climatological low-level easterly flow is the strongest (cf. Figs. 4b and 4a). The consequences of such an increment are depicted schematically in Fig. 2. The systematic reduction of the low-level flow by the analysis increments would yield weaker near-surface easterlies, and, therefore, the weaker easterly surface wind stress over the following 12-h forecast would not necessarily be balancing the vertically integrated zonal momentum tendencies derived from the analysis state.

The historical evolution of the DJF-averaged zonal wind analysis increments on the 900-hPa level (Fig. 4e) demonstrates that these increments are extremely systematic—they are there throughout the whole historical time period and are not obviously impacted by changes to observing systems, such as the inclusion of scatterometer winds in the assimilation system in the early 1990s (Dee et al. 2011). It should be noted that this is not true of MERRA (Fig. A2) where the impact of changes in observing systems is more apparent [this has also been noted in other fields (Trenberth et al. 2011)].

We can assess the extent to which we believe the near-surface flow is being correctly constrained by these analysis increments by comparing the ERA-Interim 10-m zonal winds over oceans with those from the in situ or satellite products (Fig. 5). Much like for τ_u, the CMIP5 models have stronger easterly near-surface winds than any of the observational products. ERA-Interim and MERRA compare well with the scatterometer-based products, and, if anything, the in situ WASWind measurements suggest that the 10-m winds should be even weaker than those present in ERA-Interim.[2] This indicates that, indeed, the analysis increments are acting to correctly constrain the low-level winds to be less easterly. Without this constraint, the ERA-Interim winds would likely be more easterly than the observational products and, therefore, more similar to the CMIP5 models.

Overall, this motivates the following hypothesis: some form of process that should act to reduce the strength of the near-surface easterlies is missing in the underlying forecast model of the reanalysis. This same process is likely also missing from the CMIP5 models, leading to their near-surface easterlies being faster, and their surface wind stress being stronger, than observed products. An understanding of what this missing process is could not only help improve the underlying forecast model of ERA-Interim but also help improve models in general.

b. *Evidence for a missing/erroneous process in the lower troposphere*

The inference from the above is that these analysis increments are continually acting to correct for an error that arises over the course of the 12-h forecast. The fast time scales on which these increments arise is suggestive of a missing physical process that is local to low levels in the NH low latitudes, but there is also the possibility of nonlocal influences that could act on a 12-h time scale. So, here we discuss the lines of evidence that argue for the increments primarily representing an error in processes local to the low levels of the NH low latitudes.

First, very similar structures to those seen in Fig. 4 are seen in ECMWF's operational forecast initial tendency errors (not shown). These errors occur in the very first time steps of forecast integrations, over which time nonlocal influences have not yet had a chance to be felt. But, second, additional evidence can also be obtained from the meridional wind analysis increments. Consider the rather systematic v increments, shown in Fig. 4d.

[2] Note that the SCOW and IFREMER winds are 10-m equivalent neutral winds (Liu and Tang 1996), whereas the other products are not. This could create some differences between them, but in the low latitudes, which are typically in a weakly unstable regime, the 10-m neutral and 10-m winds typically differ by less than a few tenths of $1\,\mathrm{m\,s^{-1}}$ (Mears et al. 2001).

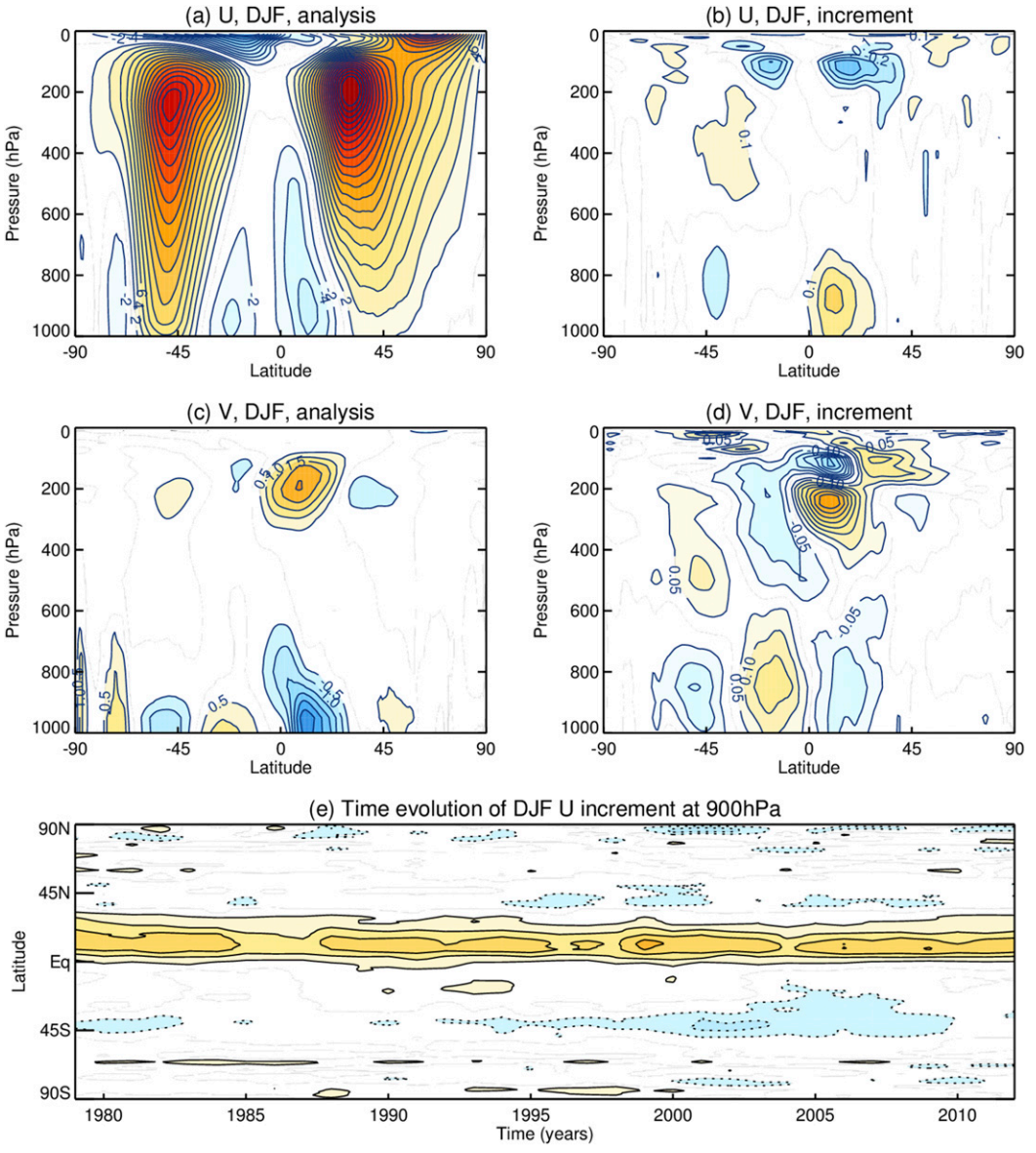

FIG. 4. ERA-Interim 1979–2005 DJF climatologies. (a) Zonal-mean zonal wind of the analysis state (contour interval is 2 m s^{-1} with the zero contour omitted), (b) zonal-mean zonal wind analysis increments (i.e., analysis state − forecast state; contour interval is 0.1 m s^{-1} with the zero contour omitted). (c),(d) As in (a),(b), but for meridional wind with contour intervals of 0.5 and 0.05 m s^{-1} respectively. (e) The yearly evolution of the DJF averaged zonal-mean zonal wind increment on the 900-hPa level [same contour interval as in (b)].

During the NH winter, the Hadley circulation is strongest in the NH as depicted by the upper-level southerlies between the equator and 30°N and the lower-level northerlies below in Fig. 4c. The analysis increments act to strengthen the upper-tropospheric southerlies and the lower-tropospheric northerlies (i.e., strengthen the Hadley circulation). Note that this increment is not small; it amounts to a strengthening of the upper-level northerlies by about 25% of the analysis climatology at 10°N and 250 hPa.

The $\overline{v}$ increments are inconsistent with the missing westerly forcing being in the upper troposphere. In the upper troposphere, around 200 hPa, the leading order balance is between the westerly tendency from $f\overline{v}$ (i.e., the Coriolis force on the meridional wind) and the easterly tendency from the combination of the other terms on the RHS of (1). An additional westerly forcing on the RHS of (1) would, therefore, be expected to be accompanied by a reduction in southerly upper-tropospheric $\overline{v}$ (i.e., a weakening of the Hadley circulation). This would be

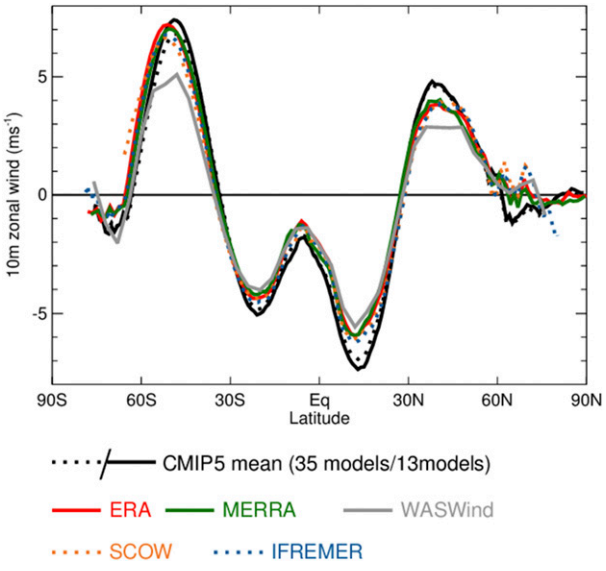

FIG. 5. DJF climatologies of zonal-mean (over ocean grid points) 10-m zonal wind for the CMIP5 models and the observation-based products.

accompanied by a weakening of the low-level northerlies and a weakening of the associated trade winds. If the forecast model were indeed missing this westerly tendency, then it would forecast easterly trades that are too strong, and the analysis increments would act to reduce them. But it would also forecast a Hadley circulation that was too strong, and the increments would be expected then to weaken the Hadley circulation, the opposite of what is seen.

The fact that the analysis increments act to strengthen the Hadley circulation while weakening the trade winds is also inconsistent with the potential influence of erroneous convective heating in the ascending branch of the Hadley circulation being the primary cause of the trade wind strength deficiency. Erroneous convective heating would have to lead to the altered trade wind strength through the mean meridional circulation, and therefore, the forecast drift in the mean meridional circulation would have to be in the sense to drive the strengthening of the easterly trade winds (i.e., the Hadley circulation would have to strengthen over the forecast, and the analysis increments would oppose this by weakening it again, the opposite of what is seen).

Instead, the zonal and meridional wind increments are both consistent with there being a missing westerly tendency in the lower troposphere, whether it is from surface drag or some other process. The lower troposphere is predominantly in an Ekman balance between the westerly tendency from boundary layer turbulence and the easterly tendency from the Coriolis force on the low-level northerlies $f\overline{v}$. A missing westerly tendency in the lower troposphere would be expected to result in increased low-level easterlies and reduced low-level northerlies over the forecast. The analysis increments would then oppose these erroneous forecast drifts through some combination of reduction of the low-level easterlies and enhancement of the low-level northerlies, which is precisely what is seen in Figs. 4b and 4d.

In summary, the combined information from the u and v increments is indicative of a missing/erroneous process at low levels that amounts to a missing westerly tendency on the zonal flow. Our hypothesis for the combined behavior of the u and v increments is that the lack of this westerly tendency leads to an enhanced low-level easterly wind and reduced low-level northerly flow over the course of the forecast evolution. The reduced northerly flow at low levels would result in reduced low-level equatorial convergence and associated reduced upper-level divergence above. Consequently, there would be an additional weakening of the upper-level southerlies of the Hadley cell, plus associated weakening of the meridional circulation in the SH. The analysis increments are then acting to oppose these erroneous drifts by strengthening the Hadley circulations again and weakening the low-level easterlies. Similar arguments, but with reversed sign, were put forward by Polichtchouk and Shepherd (2016) for the initial circulation response to an instantaneous reduction in the surface drag coefficient at low wind speeds in their model experiments.

c. *The spatial structure of the low-level analysis increments*

The spatial structure of the zonal wind analysis increments (Fig. 6b) demonstrates that the westerly increments in the NH low latitudes are occurring primarily over the ocean. Virtually all oceanic regions in the easterly trades are characterized by a westerly increment, but there are localized regions where the increments are larger than elsewhere. These might partly reflect regions with a prevalence of observations as well as regions where the forecast model is particularly erroneous.

In addition to the westerly increments in the NH low latitudes, there are weak easterly increments in the region of maximum westerlies in the extratropical Pacific, plus westerly increments in the slanted tongues of easterly flow in the SH low-latitude eastern Pacific and Atlantic (cf. Figs. 6a and 6b). In the Southern Ocean, the analysis increments do not play much of a role, but it is possible that this reflects a lack of observations to constrain the flow there, as opposed to the forecast model being without error. Indeed, with the advent of satellite scatterometer data, enhanced easterly mean analysis increments are seen in the SH westerlies (not shown).

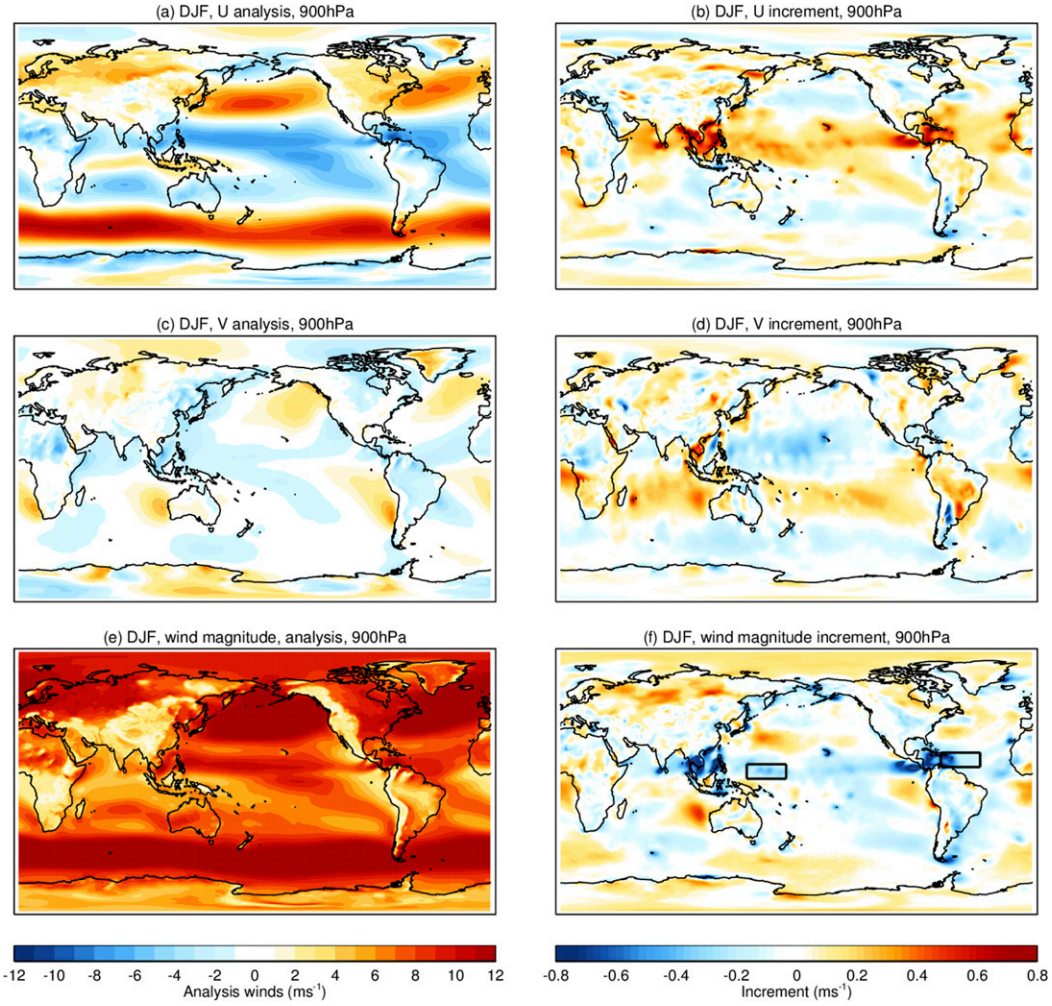

FIG. 6. Climatology of the (left) analysis state and (right) analysis increment. Shown are 900-hPa DJF climatologies from 1979–2005 for (a),(b) zonal wind, (c),(d) meridional wind, and (e),(f) scalar wind speed. [Boxes in (f) denote the regions used in Fig. 10.]

With the exception of the Southern Ocean, it does appear that the zonal wind analysis increments in general act to oppose the low-level flow, which is indicative of a missing drag on the low-level zonal winds. This can be summarized through the correlation between the climatological zonal wind increment and the climatological forecast wind at each ocean grid point (north of 30°S) (Fig. 7a). They are correlated, with regions of easterly climatological wind experiencing westerly increments and vice versa.

The meridional wind increments (Fig. 6d), in contrast, do not oppose the meridional wind climatology. Instead, they are characterized by a rather zonally symmetric strengthening of the northerlies in the NH low latitudes and the southerlies in the SH low latitudes (i.e., the strengthening of the Hadley circulations previously discussed).

The zonal wind increments are consistent with the surface drag being too weak in that they generally oppose the zonal wind climatology. The meridional wind increments are also consistent with a missing surface drag when one considers the Ekman meridional wind that would arise from insufficient drag on the zonal flow, as discussed above. Indeed, the net effect of the increments on the wind magnitude (i.e., u and v combined) in the NH low latitudes is to weaken the surface winds as can be seen in Figs. 6e and 6f.

Overall, the analysis increments paint a picture of the drag on the low-level flow being too weak in the forecast model. To counteract this, the increments act to weaken the easterly trades, as well as oppose the drift in the meridional wind that would arise through the Ekman balance response to the missing drag on the zonal flow. In the following section, this hypothesis is further

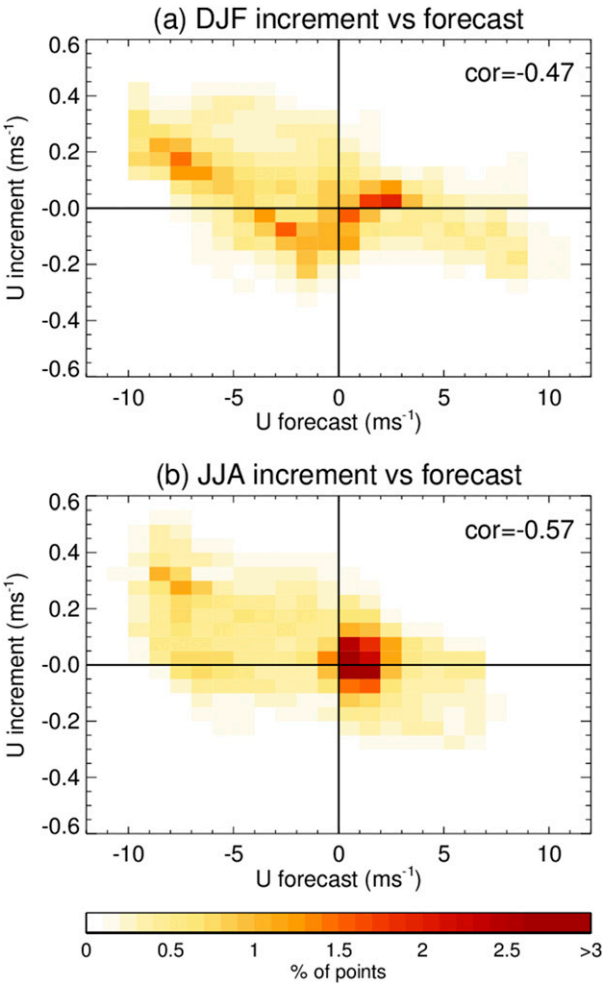

FIG. 7. Joint probability distribution (across ocean grid points north of 30°S) of the climatological zonal wind analysis increment against the climatological forecast zonal wind on the 900-hPa level. (a) DJF and (b) JJA. The correlation between the analysis increment and the forecast is noted in the top right-hand corner. Points south of 30°S are omitted because the analysis increments do not play a major role in that region.

supported by the behavior of the analysis increments in June–August (JJA).

6. The momentum balance and analysis increments during SH winter

Our focus, so far, has been on the NH wintertime trade winds, motivated by the large discrepancies in τ_u between the models and reanalyses. But, in fact, there is a role for the analysis increments during the SH winter as well. During SH winter, the easterly trades maximize in the SH low latitudes. Turning back to Fig. 3g, it can be seen that, in the SH winter, the easterly surface wind stress in the SH low latitudes is also weaker in ERA-Interim than in the models, although not to the same degree as in the NH. Again, at least in the low latitudes north of around 20°S, the vertically integrated resolved dynamics tendencies in the models are very comparable to those in the reanalysis (i.e., the difference in Fig. 3h is small), and a residual exists in the ERA-Interim momentum balance (Figs. 3f,i) that is of similar magnitude to the τ_u discrepancy between CMIP5 and ERA-Interim (Fig. 3g).

Considering now the analysis increments on the zonal-mean u and v during JJA (Fig. 8), a somewhat mirror image of the NH increments is found (cf. with Fig. 4). In JJA, the easterly trades are strongest in the SH low latitudes between 30°S and the equator, and here there are westerly increments in the lower troposphere that act to weaken these easterlies. Accompanying this, the increments also act to strengthen the Hadley cells in both hemispheres, much like during DJF.

A comparison of the spatial patterns of 900-hPa climatological flow and analysis increments during JJA (Figs. 9a and 9b) lend strong support to the hypothesis that the increments are acting as an extra drag on the low-level flow because here, in the region of strong low-level westerlies in the Asian monsoon inflow, the analysis increments are easterly, whereas elsewhere, in the regions of strong easterly trade winds, they are westerly. The climatological zonal wind analysis increments and forecast winds are, again, correlated over ocean grid points as summarized in Fig. 7b, the meridional wind increments appear to be counteracting the Ekman meridional flow that would be induced by the lack of zonal drag (Fig. 9d), and the net effect is still a reduction in wind magnitude in the regions that exhibit strong climatological winds such as the northern and southern Indian Ocean and the Pacific in the southern low latitudes and in the vicinity of Hawaii (Fig. 9f). The momentum balance and analysis increments during JJA, therefore, are also consistent with there being a missing drag on low-level winds over the ocean. It should be noted that ERA-Interim and MERRA do differ in some regards in the SH as discussed more in appendix A.

7. Discussion

A number of pieces of evidence have been presented that support the hypothesis that there is a missing drag on the low-level zonal flow over oceans in GCMs. These can be summarized as follows:

- The CMIP5 models rather consistently exhibit stronger zonal-mean zonal surface wind stress and near-surface winds than reanalyses and other observation-based products in the NH low latitudes during winter.
- The momentum balance calculation, however, shows that this difference in τ_u cannot be attributed to a difference in either the resolved dynamics terms or

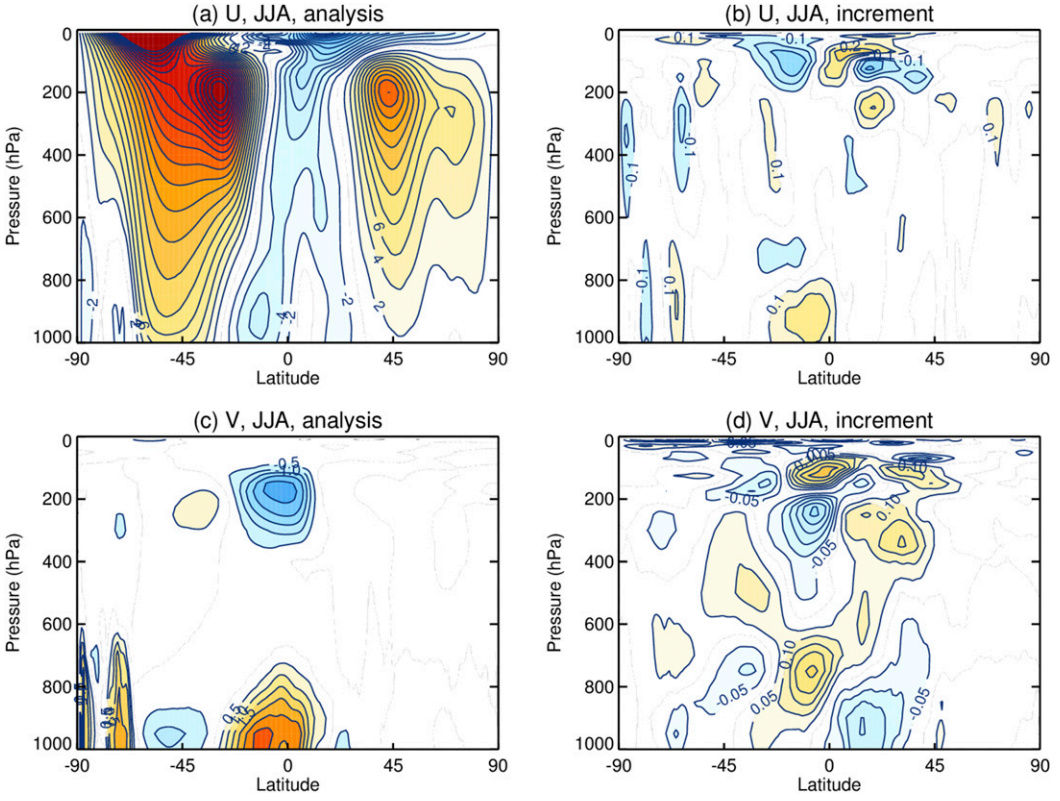

FIG. 8. ERA-Interim 1979–2005 JJA climatologies. (a) Zonal-mean zonal wind of the analysis state (contour interval is 2 m s^{-1} with the zero contour omitted), (b) zonal-mean zonal wind analysis increments (i.e., analysis state − forecast state; contour interval is 0.1 m s^{-1} with the zero contour omitted). (c),(d) As in (a),(b), but for meridional wind with contour intervals of 0.5 and 0.05 m s^{-1} respectively.

the other parameterized tendencies within the free atmosphere. The sum of these vertically integrated tendencies in the reanalyses would be balanced by a stronger westerly $-\tau_u$ than is present, and, as a result, the momentum balance in reanalyses does not add up.

- The mean analysis increments were found to play an important role. They rather systematically act to reduce the near-surface zonal-mean easterly trades during NH winter, bringing them close to independent observational products and resulting in a weaker zonal-mean τ_u than the forecast model would otherwise produce.
- Systematic increments in the meridional wind can help to rule out the possibility of the missing westerly tendency being in the upper troposphere and support the role of the low-level zonal wind increments in accounting for a model error near the surface.
- The seasonal and spatial variations of the analysis increments provide strong support for a missing drag on the low-level zonal flow; that is, the zonal wind increments rather consistently act to oppose the climatological zonal flow in both hemispheres and seasons.

If models are missing a drag on the low-level flow, then there are two distinct possibilities to consider: 1) there is something incorrect in our formulation of the drag between the atmosphere and the ocean surface, or 2) there is some other missing process that does not represent a drag between the atmosphere and the surface but represents some other form of momentum transfer within the atmosphere itself. It is important to distinguish between these two possibilities as they would have rather different interpretations and consequences for the coupled ocean–atmosphere system.

In the case of option 1, the momentum imbalance and analysis increments would suggest that the drag, from the surface, on the low-level winds is too weak. The problem cannot lie in the vertical diffusion of momentum within the atmosphere itself because this would provide no net vertically integrated westerly tendency and therefore would not help with the reanalysis momentum imbalance problem. Instead, it would have to be the surface drag between the atmosphere and ocean that is in error. The momentum balance discrepancies and analysis increment behavior could be easily reconciled by the surface drag, associated with a given wind

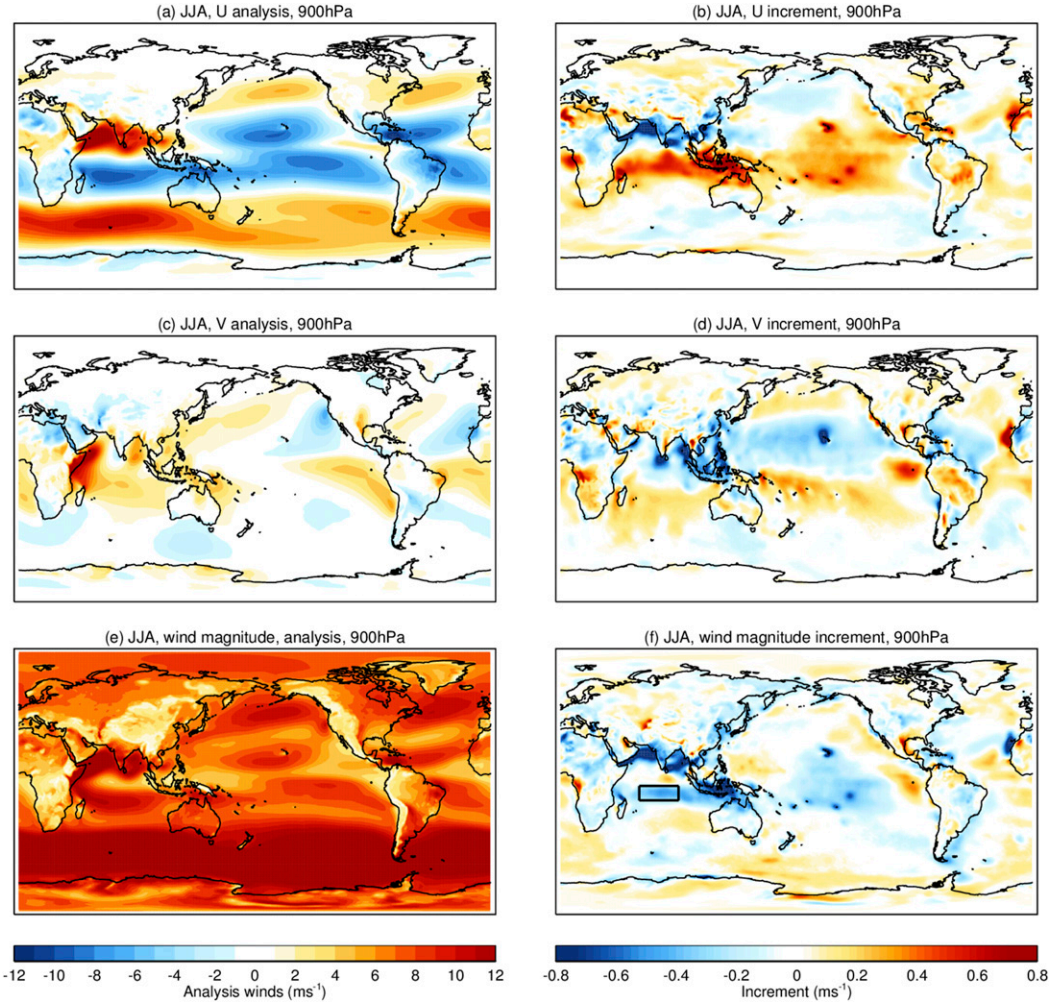

FIG. 9. As in Fig. 6, but for JJA.

speed, being too weak. A stronger surface drag, for a given wind speed, in the underlying forecast model of the reanalyses would maintain a weaker low-level flow, and the zonal wind increments would no longer need to play that role. Furthermore, the momentum balance in the reanalyses would add up, because the weak, real-world, near-surface winds would be associated with a stronger surface wind stress that could then balance the strong easterly forcings coming in from the resolved dynamics and parameterized tendencies above. The implications of this, however, would be that the observation-based surface wind stresses in the NH low latitudes, and likely elsewhere, are also too weak. While it is unintuitive to conclude that it may be the observational τ_u estimates that are in error, it is certainly conceivable given that all the wind stress products rely on the same formulation as the models for the representation of surface drag in terms of the near-surface winds and stability [see (5) in section 2b]. From the scatterometer and in situ measurements we have evidence that the near-surface winds in the reanalyses are reasonable, but if our formulation of the surface drag is incorrect, the stresses derived from these winds may not be, and the momentum budget analysis would suggest that the real-world NH low-latitude τ_u should be more easterly.[3] The implications of this for the CMIP5 models would then be that their τ_u representation in the NH low latitudes is not necessarily incorrect, but they are

[3] This assumes that the resolved circulation of the reanalysis and the associated momentum transport terms are adequately constrained by observations. This is not something that is easy to assess, but given that there is a clear role for the increments to provide a constraint on the large-scale flow in both the upper and lower troposphere, and the momentum balance terms in ERA-Interim and MERRA compare well, at least in the NH, it seems reasonable to assume that this is the case.

obtaining it for the wrong reasons, with near-surface winds that are too fast.

The implications of option 2 would be rather different. Option 2 would require there to be some missing momentum transfer within the atmosphere that acts to reduce the low-level flow. Then both the near-surface winds and the surface wind stress in the reanalysis would be correct, as the increments would be playing the role of this process. This missing process would amount to a net westerly tendency on the RHS of (4) in the NH low latitudes during DJF, allowing the momentum balance to add up. Both the near-surface winds and the surface wind stress in the CMIP5 models would then be in error, and this would have implications for the ocean circulation in such coupled models.

We can speculate on processes that could be misrepresented under either possibility. In terms of a misrepresentation of the drag between the surface and the atmosphere (option 1), for one thing, the neutral drag coefficients C_{DN} derived from observations are uncertain (Edson et al. 2013), and these results may simply be suggesting that models should be pushing their drag coefficients to the upper limit of this uncertainty. Indeed, preliminary analysis (not shown) suggests that initial tendency errors on the zonal wind in ECMWF's operational forecasts can be reduced by increasing C_{DN} within reasonable bounds. Another possibility is that the effects of subgrid-scale deep convection and associated cold pools on gustiness and boundary layer turbulence are not being adequately represented by current gustiness parameterizations that are intended to represent such effects (e.g., Zeng et al. 2002, and references therein). Indeed, the analysis increments that act to reduce the magnitude of the low-level flow are predominantly in the low latitudes where deep convection is prevalent. It is conceivable that these effects are also inadequately represented in the reanalyses as well as in the observation-based products where surface wind stresses are typically derived from daily averaged 10-m winds using the bulk formulations discussed in section 2b.

In terms of a misrepresentation of a momentum transfer process within the atmosphere itself (option 2), one possibility is the neglect of wind turning between the lowest model level and the surface. It is assumed that the drag exerted on the atmosphere is in the opposite direction to the flow on the lowest model level, but, in reality, over the finite distance between the surface and that level, the boundary layer turbulence may induce some turning of the wind vector (Svensson and Holtslag 2009). In the NH low latitudes, this would be in the sense that flow at the surface would have more of a northerly component at the expense of the easterly component, which is in the sense required to explain the analysis increments (G. Svensson 2017, personal communication).

These are all possibilities to consider in the future. An initial exploration of the atmospheric regimes within which the analysis increments arise is presented in Fig. 10. These joint probability distribution functions are constructed from all 12-h forecasts at each grid point within three localized regions: the low-latitude Atlantic during DJF, the low-latitude west Pacific during DJF, and the low-latitude Indian Ocean during JJA (see the rectangular regions in Figs. 6f and 9f where the mean wind speed increments are particularly negative). Figures 10a–c show the dependency of the 10-m scalar wind speed analysis increment on the instantaneous 10-m scalar wind speed of the forecast state. These tell us that the wind speed range of relevance is between 4 and 12 $\mathrm{m\,s^{-1}}$. This is within the intermediate wind speed range, over which C_{DN} is most observationally constrained, but there is an observational uncertainty nonetheless (Edson et al. 2013, their Fig. 6). On an instantaneous basis, the correlation between wind speed and wind speed increment is not particularly strong, although it is predominantly negative in each region (see the values in the top right of each panel of Fig. 10). A negative correlation would be expected if C_{DN} were too small, and it may be that there are too many other, less systematic, factors that give rise to increments on an instantaneous basis for this relationship to explain a large fraction of the variance in scalar wind speed increments. Figures 10d–f show the dependency of the 10-m scalar wind speed increments on the forecast average surface buoyancy flux (calculated from the sensible and latent heat fluxes), which is an indicator of near-surface stability. This shows that the regions of interest are typically in a weakly unstable regime (negative buoyancy flux) and that there is no consistent correlation between the occurrence of the analysis increments and the near-surface stability.

This preliminary analysis, while telling us the typical wind speeds and stabilities in the regions of interest, also indicates that there may be too many other, less systematic, factors contributing to the analysis increments on an instantaneous basis for a deeper investigation into the dependence on different atmospheric regimes to be fruitful. Instead, a more targeted modeling approach may be the best way forward. This approach should aim to systematically investigate the improvements that can be obtained through considering each of the possibilities discussed above, paying attention not only to the momentum balance aspects of the climatology but also to the thermodynamic aspects, such as precipitation and evaporation, which will likely be affected by any

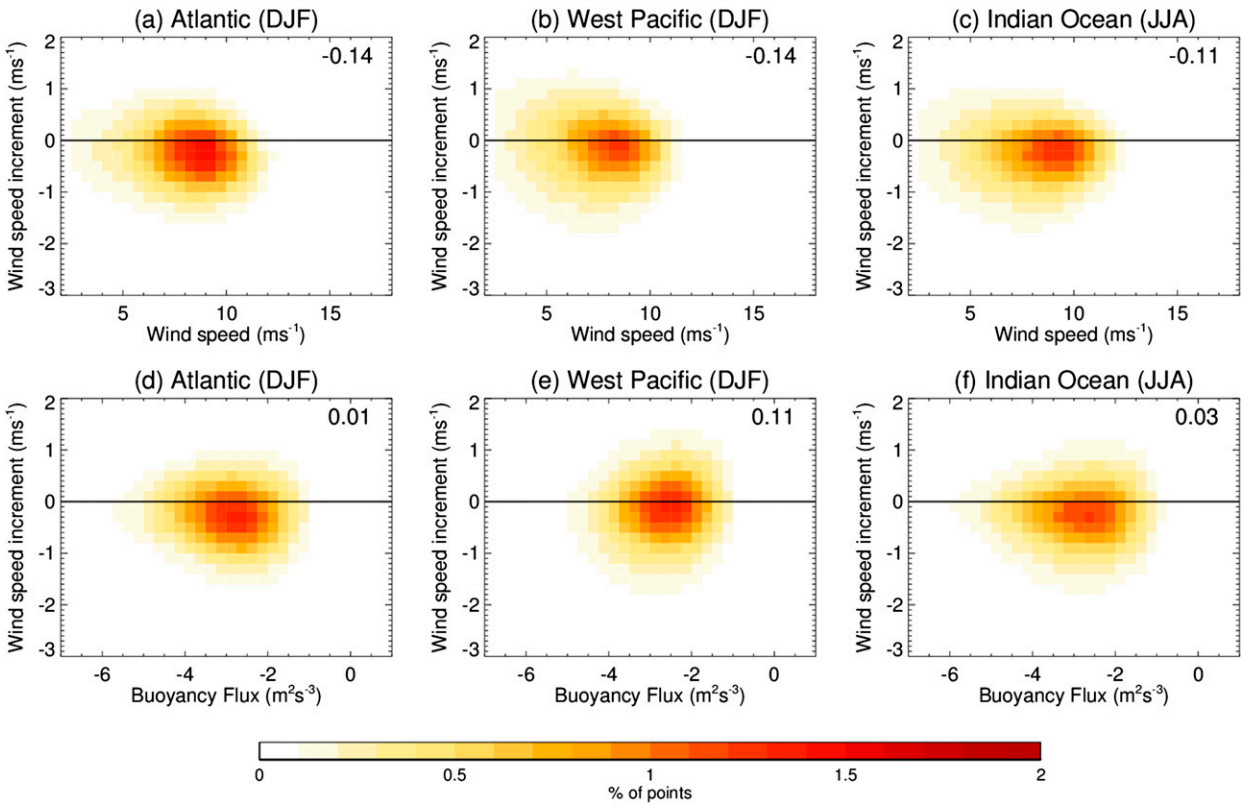

FIG. 10. Joint probability distribution functions of the analysis increment on the 10-m scalar wind speed vs (top) the forecast 10-m scalar wind speed and (bottom) the forecast surface buoyancy flux. These are the distributions over all temporal and spatial points within a box in the (a),(d) low-latitude North Atlantic during DJF, (b),(e) low-latitude western North Pacific during DJF, and (c),(f) low-latitude south Indian Ocean during JJA. These boxes are shown in Figs. 6f and 9f.

modifications that are made. This may help to disentangle what is the ultimate near-surface process misrepresentation that is leading to the surface wind stress discrepancies discussed here.

Acknowledgments. We thank three anonymous reviewers for their helpful comments. This work was funded by National Science Foundation funding to the National Center for Atmospheric Research. Isla Simpson is grateful to Kevin Trenberth, Gunilla Svensson, and Jenny Lindvall for helpful comments on the manuscript as well as Bill Large, Justin Small, Steve Yeager, Dudley Chelton, and Ralph Millif for helpful discussions on different aspects of this work and Richard Seager and Tiffany Shaw for discussions on the momentum balance calculation. We acknowledge the World Climate Research Programme's Working Group on Coupled Modelling, which is responsible for CMIP, and we thank the climate modeling groups (listed in Table 1 of this paper) for producing and making available their model output. For CMIP the U.S. Department of Energy's Program for Climate Model Diagnosis and Intercomparison provides coordinating support and led development of software infrastructure in partnership with the Global Organization for Earth System Science Portals. ERA-Interim data were provided courtesy of ECMWF. MERRA was developed by the Global Modeling and Assimilation Office and supported by the NASA Modeling, Analysis and Prediction Program. Source data files can be acquired from the Goddard Earth Science Data Information Services Center (GES DISC).

APPENDIX A

Momentum Balance and Analysis Increments in MERRA

To demonstrate that the results in the main body of the text are not solely representative of ERA-Interim, we present results from MERRA for comparison. ERA-Interim was chosen over MERRA for the main discussion, because 1) there are a wider variety of roles for the analysis increments in the climate of MERRA reanalysis, suggesting a wider range of issues in the underlying forecast model, and 2) it has been demonstrated (deWeaver and Nigam 1997) that the assimilation

procedure used in MERRA is less able to correctly constrain the divergent circulation. Nevertheless, the behavior of MERRA is broadly consistent with ERA-Interim and lends support to the main conclusions drawn.

MERRA is created using incremental analysis updates (IAUs) (Bloom et al. 1996). As such, there are two types of products available for MERRA: the ''ana'' products, which refer to an analysis state in the same sense as ERA-Interim (i.e., the optimal combination of the forecast state and assimilated observations), and the ''asm'' products, which refer to the output from a model simulation with the IAUs imposed as tendency terms to the prognostic equations. These IAUs are the difference between the ana state and the forecast state converted to a tendency (i.e., the analysis increments converted to a tendency). The asm state offers the advantage that the resolved and parameterized tendencies combined with the IAU tendencies should balance to the same degree that the free-running CMIP5 models do, and so we show the balance here using the asm fields. Since the MERRA analysis increments are provided as tendencies ($m\,s^{-2}$) as opposed to analysis − forecast differences, we multiply these tendencies by the number of seconds in 12 h for comparison with the ERA-Interim analysis increments.

Much like for ERA-Interim (Fig. 3g), MERRA exhibits greater easterly surface wind stress in the NH low latitudes than CMIP5 (Fig. A1d). North of 10°N, the vertically integrated resolved dynamics terms are, again, rather similar between CMIP5 and MERRA and cannot explain this difference in τ_u (Figs. A1b,e vs Fig. 3b). However, unlike ERA-Interim, MERRA does exhibit weaker easterly resolved dynamics tendencies than CMIP5 in the lowest latitudes (equatorward of 10°N; Fig. A1e); that is, there is disagreement between ERA-Interim and MERRA in the resolved dynamics tendencies here.

A substantial residual exists in the vertically integrated momentum balance of MERRA in the NH low latitudes, even when the parameterized tendencies are included (Fig. A1f). Quantitatively, the MERRA τ_u at 14°N is $-0.067\,N\,m^{-2}$, whereas the stress that is required to balance the resolved dynamics and parameterized tendencies is $-0.098\,N\,m^{-2}$, which is much closer to the CMIP5 value of $-0.107\,N\,m^{-2}$. Much like for ERA-Interim, this indicates the important role that the analysis increments play. For the MERRA asm fields we can examine the vertically integrated tendency from these analysis increments (Fig. A1g), and it does, indeed, constitute a vertically integrated westerly tendency that cancels out this residual (Fig. A1h).

The zonal-mean zonal and meridional wind analysis increments during DJF (Fig. A2) can be compared with the ERA-Interim equivalent in Fig. 4. In general, the increments seem to play a wider range of roles than in ERA-Interim, but in the NH low latitudes, the increments are acting to reduce the low-level easterly flow, in much the same way as in ERA-Interim. Associated with this is a tendency for the increments to weaken the low-level northerlies and enhance the upper-level southerlies, although this effect is more meridionally confined than in ERA-Interim. In contrast to ERA-Interim, there is some evolution over time in the prevalence of these low-level westerly increments (Fig. A2e). The increments are stronger from the late 1990s onward, which may have something to do with the introduction of *European Remote Sensing Satellite-2 (ERS-2)* scatterometer winds in 1996 and QuikSCAT winds in 1999 to the assimilation system (Rienecker et al. 2011). Similar drifts in the behavior of MERRA over time have been noted by Trenberth et al. (2011) in the context of global precipitation and energy balances.

The spatial structure of the 900-hPa zonal wind and zonal wind increments for DJF and JJA (Fig. A3) can be compared with the ERA-Interim equivalents in Figs. 6 and 9. Motivated by the time evolution of the increments in Fig. A2e, Figs. A3c and A3f show the climatological analysis increments for the 1998–2015 period separately. Again, there are a wider variety of features seen in the analysis increments for MERRA, such as the greater prevalence of increments over land. But nevertheless, they do support the conclusions derived from ERA-Interim. During the NH winter, the increments impart westerly tendencies on the flow in the NH low latitudes. When the full time period is considered, the influence of these increments is more restricted to the west Pacific, Indian Ocean, Hawaii, and Atlantic, perhaps related to the locations at which observations are available. When only the post-1998 period is considered, however, it can be seen that westerly increments are present over a wider expanse of the ocean surface, perhaps related to the increased assimilation of scatterometer winds.

Similarly, during NH summer, MERRA exhibits broadly similar features to those in ERA-Interim, with the increments acting to reduce the strength of the easterly trades in the SH low latitudes and reduce the strength of the westerly monsoon inflow in the Indian Ocean. While there is a clear tendency for the increments to reduce the easterly trades in the SH, MERRA does differ from ERA-Interim in the vertically integrated momentum balance there. MERRA exhibits slightly weaker easterly wind stress in the SH than ERA-Interim [apparent from a comparison of the differences with CMIP5 (Figs. 3g and A1d)]. It also exhibits a weaker net easterly tendency from the resolved dynamics tendencies than ERA-Interim (cf. Figs. 3h and

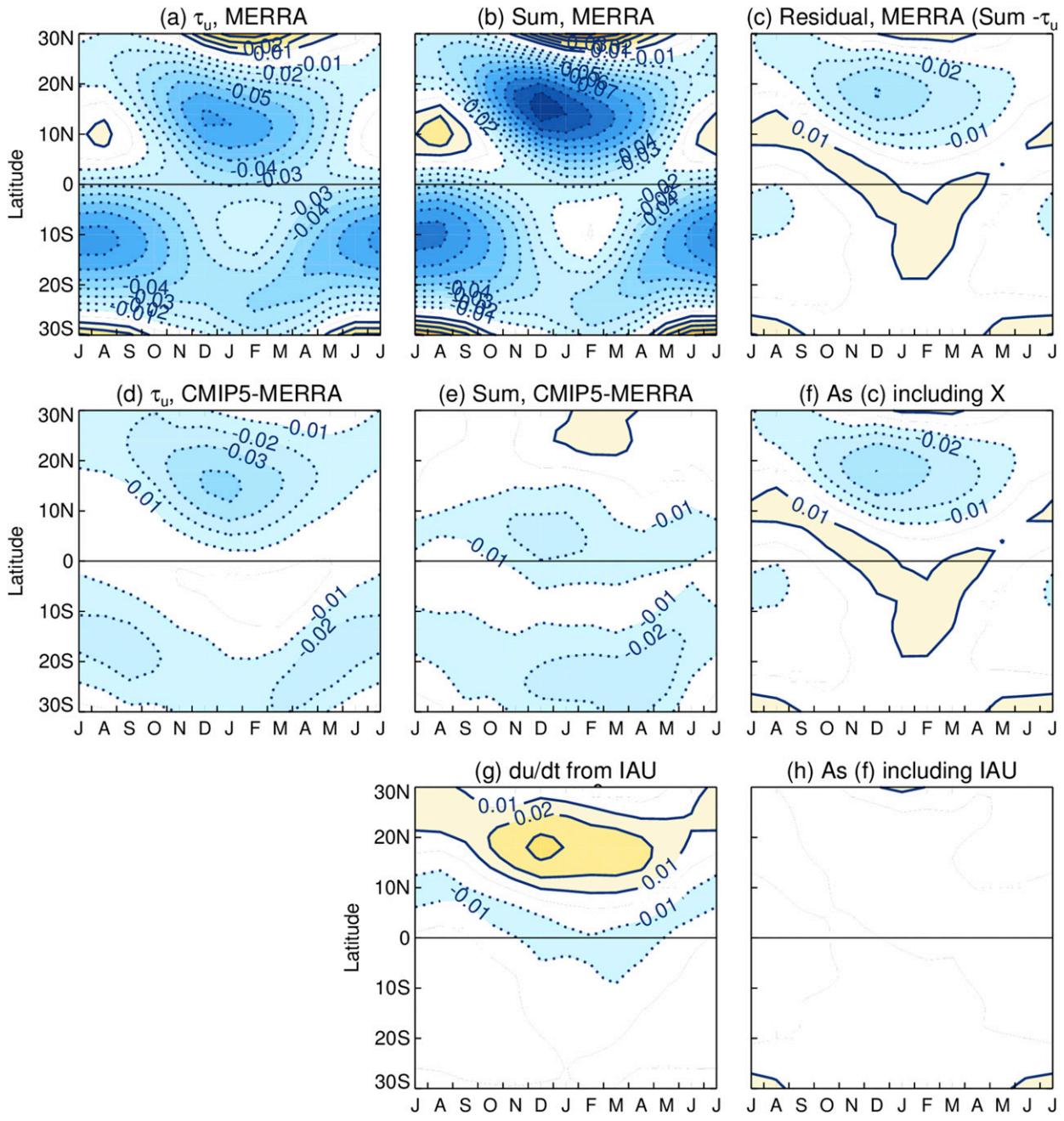

FIG. A1. The momentum balance for the MERRA reanalysis: (a) τ_u, (b) the resolved dynamics terms, and (c) the residual between them. (d) The difference in τ_u between CMIP5 and MERRA, (e) the difference in the resolved dynamics terms between CMIP5 and MERRA, and (f) the MERRA residual when other parameterized tendencies are included. (g) The tendencies from the IAUs and (h) the residual when the IAUs are included in the balance.

A1e). While the increments are acting to reduce the low-level easterlies in the SH, they are also providing an easterly tendency above, and, therefore, their vertically integrated contribution is minimal. Given the differences in the resolved tendencies between ERA-Interim and MERRA in the SH, it is difficult to draw firm conclusions about the fidelity of the resolved dynamics terms in CMIP5 models there, since they compare well with ERA-Interim but differ from MERRA.

In summary, while some differences do exist between MERRA and ERA-Interim, the analysis increments in MERRA act to reduce the low-level zonal flow in a similar fashion, indicating a missing drag on the low-level flow in the underlying forecast model and lending

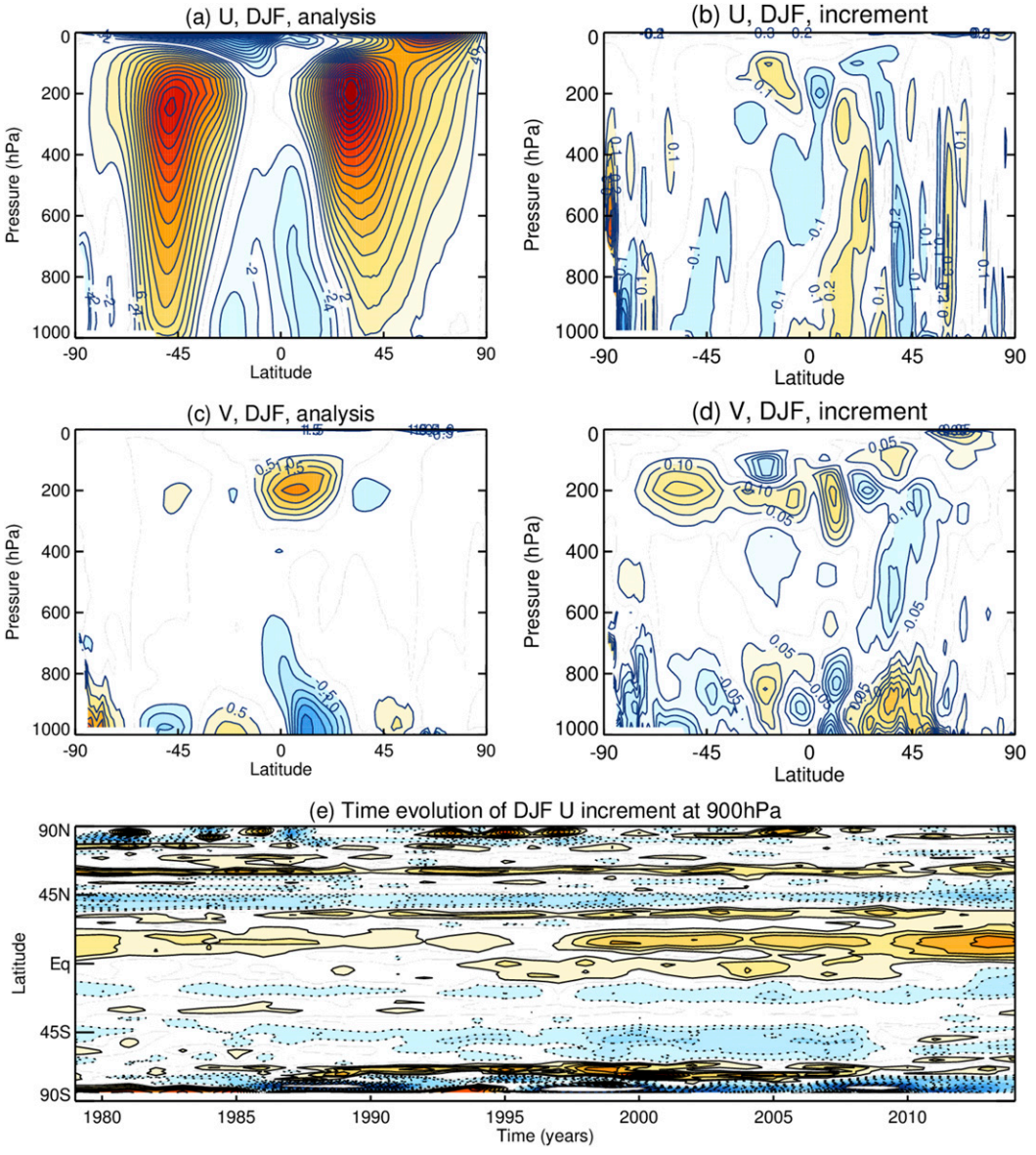

FIG. A2. As in Fig. 4, but for MERRA. The climatologies in (a)–(d) are calculated for the 1979–2015 period.

support to the overall conclusions drawn from ERA-Interim in the main body of the text.

APPENDIX B

Description of Additional Observation-Based Datasets

In addition to the two reanalysis datasets, we make use of a variety of observation-based datasets of surface wind stress, 10-m winds, and 10-m neutral winds as summarized in Table 2. Below is a brief description of each of these datasets.

- COREv2 τ_u (Large and Yeager 2009): This dataset provides a historical estimate of surface fluxes of momentum, heat, and moisture. These surface fluxes are obtained using bulk formulas [e.g., (5)] but with the input near-surface fields derived from observations. While the primary input dataset of winds, temperature, specific humidity, and density is the NCEP reanalysis, these data are first corrected to account for known biases using a wide range of in situ and satellite-based observations such as buoy measurements of near-surface temperature and QuikSCAT vector winds. In addition, this dataset is self-consistent overall, in that the fluxes of momentum and latent and sensible heat are all calculated using the

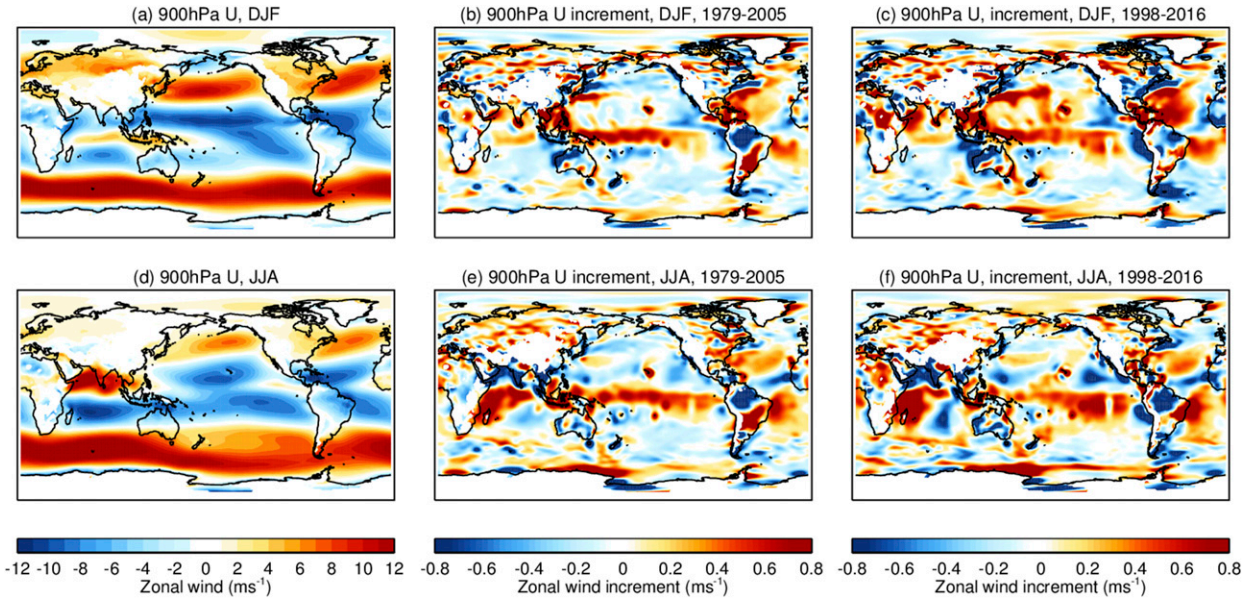

FIG. A3. MERRA DJF climatologies on the 900-hPa level. (a) DJF-averaged zonal wind climatology (1979–2015), (b) climatological zonal wind increment (1979–2005), and (c) climatological zonal wind increment for the 1998–2015 period. (d)–(f) As in (a)–(c), but for JJA.

same winds, and yield only a small imbalance in the net globally averaged air–sea heat flux when combined with independent radiation and precipitation measurements. The bulk formula methodology and drag coefficients used to obtain the surface fluxes from near-surface quantities are those described in Large and Yeager (2004). We make use of the zonal surface wind stress climatology from 1979 to 2005.

- SCOW u_{10N} and τ_u (Risien and Chelton 2008): The Scatterometer Climatology of Ocean Winds is a dataset of surface wind stress and near-surface winds derived solely from QuikSCAT measurements and runs from September 1999 to August 2007. The 10-m neutral zonal winds are directly obtained through the GMF, and the calculation of τ_u assumes the Large et al. (1994) formulation of C_{DN}.
- IFREMER u_{10N} and τ_u (Bentamy et al. 2013): The IFREMER dataset also provides 10-m neutral winds and surface stress obtained from QuikSCAT. However, in comparison with SCOW, it uses a newer reprocessed version of the scatterometer retrievals, which is based on a newer GMF (Ricciardulli and Wentz 2011) and the Fairall et al. (2003) formulation of C_{DN}. This dataset runs from 1999 to 2009 with some data gaps.
- WASWind u_{10} (Tokinaga and Xie 2011): The Wave and Anemometer-Based Sea Surface Wind dataset is constructed from ship-based observations that were archived in the International Comprehensive Ocean–Atmosphere Dataset (ICOADS) and includes various bias corrections and adjustments to account for trends in anemometer heights. We make use of the WASWind 10-m zonal winds from 1979 to 2005.

REFERENCES

Andrews, D. G., J. R. Holton, and C. B. Leovy, 1987: *Middle Atmosphere Dynamics.* Academic Press, 124 pp.

Beljaars, A. C. M., A. R. Brown, and N. Wood, 2004: A new parametrization of turbulent orographic form drag. *Quart. J. Roy. Meteor. Soc.*, **130**, 1327–1347, https://doi.org/10.1256/qj.03.73.

Bentamy, A., S. A. Grodsky, K. Katsaros, M. Mestas-Nuñez, B. Blanke, and F. Desbiolles, 2013: Improvement in air–sea flux estimates derived from satellite observations. *Int. J. Remote Sens.*, **34**, 5243–5261, https://doi.org/10.1080/01431161.2013.787502.

Bloom, S., L. Takacs, A. DaSilva, and D. Ledvina, 1996: Data assimilation using incremental analysis updates. *Mon. Wea. Rev.*, **124**, 1256–1271, https://doi.org/10.1175/1520-0493(1996)124<1256:DAUIAU>2.0.CO;2.

Butchart, N., and Coauthors, 2011: Multimodel climate and variability of the stratosphere. *J. Geophys. Res.*, **116**, D05102, https://doi.org/10.1029/2010JD014995.

Chen, G., I. M. Held, and W. Robinson, 2007: Sensitivity of the latitude of the surface westerlies to surface friction. *J. Atmos. Sci.*, **64**, 2899–2915, https://doi.org/10.1175/JAS3995.1.

Dee, D. P., and Coauthors, 2011: The ERA-Interim reanalysis: Configuration and performance of the data assimilation system. *Quart. J. Roy. Meteor. Soc.*, **137**, 553–597, https://doi.org/10.1002/qj.828.

deWeaver, E., and S. Nigam, 1997: Dynamics of zonal-mean flow assimilation and implications for winter circulation anomalies. *J. Atmos. Sci.*, **54**, 1758–1775, https://doi.org/10.1175/1520-0469(1997)054<1758:DOZMFA>2.0.CO;2.

Edson, J. B., and Coauthors, 2013: On the exchange of momentum over the open ocean. *J. Phys. Oceanogr.*, **43**, 1589–1610, https://doi.org/10.1175/JPO-D-12-0173.1.

Fairall, C. W., D. P. Bradley, D. P. Rogers, J. B. Edson, and G. S. Young, 1996: Bulk parameterization of air-sea fluxes in Tropical Ocean-Global Atmosphere Coupled-Ocean Atmosphere Response Experiment. *J. Geophys. Res.*, **101**, 3747–3767, https://doi.org/10.1029/95JC03205.

——, E. F. Bradley, J. E. Hare, A. A. Grachev, and J. B. Edson, 2003: Bulk parameterization of air–sea fluxes: Updates and verification of the COARE algorithm. *J. Climate*, **16**, 571–591, https://doi.org/10.1175/1520-0442(2003)016<0571:BPOASF>2.0.CO;2.

Garfinkel, C. I., A. M. Molod, L. D. Oman, and I.-S. Song, 2011: Improvement of the GEOS-5 AGCM upon updating the air-sea roughness parameterization. *Geophys. Res. Lett.*, **38**, L18702, https://doi.org/10.1029/2011GL048802.

Klinker, E., and P. D. Sardeshmukh, 1992: The diagnosis of mechanical dissipation in the atmosphere from large-scale balance requirements. *J. Atmos. Sci.*, **49**, 608–627, https://doi.org/10.1175/1520-0469(1992)049<0608:TDOMDI>2.0.CO;2.

Large, W. G., and S. Pond, 1982: Open ocean momentum flux measurements in moderate to strong winds. *J. Phys. Oceanogr.*, **12**, 464–482, https://doi.org/10.1175/1520-0485(1982)012<0464:SALHFM>2.0.CO;2.

——, and S. G. Yeager, 2004: Diurnal to decadal global forcing for ocean and sea ice models: The data sets and climatologies. NCAR Tech. Note NCAR/TN-460+STR, 112 pp., http://opensky.ucar.edu/islandora/object/technotes:434.

——, and ——, 2009: The global climatology of an interannually varying air-sea flux data set. *Climate Dyn.*, **33**, 341–364, https://doi.org/10.1007/s00382-008-0441-3.

——, J. C. McWilliams, and S. C. Doney, 1994: Oceanic vertical mixing: A review and a model with a nonlocal boundary layer parameterization. *Rev. Geophys.*, **32**, 363–403, https://doi.org/10.1029/94RG01872.

Lee, T., D. E. Waliser, J.-L. Li, F. W. Landerer, and M. M. Gierach, 2013: Evaluation of CMIP3 and CMIP5 wind stress climatology using satellite measurements and atmospheric reanalysis products. *J. Climate*, **26**, 5810–5826, https://doi.org/10.1175/JCLI-D-12-00591.1.

Liu, W. T., and W. Tang, 1996: Equivalent neutral wind. Jet Propulsion Laboratory Publ. 96-17, 22 pp., https://ntrs.nasa.gov/archive/nasa/casi.ntrs.nasa.gov/19970010322.pdf.

Lott, F., and M. J. Miller, 1997: A new subgrid-scale orographic drag parametrization: Its formulation and testing. *Quart. J. Roy. Meteor. Soc.*, **123**, 101–127, https://doi.org/10.1002/qj.49712353704.

McFarlane, N., 1987: The effect of orographically excited gravity wave drag on the general circulation of the lower stratosphere and troposphere. *J. Atmos. Sci.*, **44**, 1775–1800, https://doi.org/10.1175/1520-0469(1987)044<1775:TEOOEG>2.0.CO;2.

McLandress, C., T. G. Shepherd, S. Polavarapu, and S. Beagley, 2012: Is missing orographic gravity wave drag near 60°S the cause of stratospheric zonal wind biases in chemistry–climate models? *J. Atmos. Sci.*, **69**, 802–818, https://doi.org/10.1175/JAS-D-11-0159.1.

Mears, C. A., D. K. Smith, and F. J. Wentz, 2001: Comparison of special sensor microwave imager and buoy-measured wind speeds from 1987 to 1997. *J. Geophys. Res.*, **106**, 11 719–11 729, https://doi.org/10.1029/1999JC000097.

Palmer, T. N., G. Shutts, and R. Swinbank, 1986: Alleviation of a systematic westerly bias in general circulation and numerical weather prediction models through an orographic gravity wave drag parametrization. *Quart. J. Roy. Meteor. Soc.*, **112**, 1001–1039, https://doi.org/10.1002/qj.49711247406.

Pithan, F., T. G. Shepherd, G. Zappa, and I. Sandu, 2016: Climate model biases in jet streams, blocking and storm tracks resulting from missing orographic drag. *Geophys. Res. Lett.*, **43**, 7231–7240, https://doi.org/10.1002/2016GL069551.

Polichtchouk, I., and T. G. Shepherd, 2016: Zonal-mean circulation response to reduced air–sea momentum roughness. *Quart. J. Roy. Meteor. Soc.*, **142**, 2611–2622, https://doi.org/10.1002/qj.2850.

Pulido, M., 2014: A simple technique to infer the missing gravity wave drag in the middle atmosphere using a general circulation model: Potential vorticity budget. *J. Atmos. Sci.*, **71**, 683–696, https://doi.org/10.1175/JAS-D-13-0198.1.

Ricciardulli, L., and F. Wentz, 2011: Reprocessed QuikSCAT (v04) wind vectors with Ku-2011 geophysical model function. Remote Sensing Systems Tech. Rep. 043011, 8 pp., http://images.remss.com/qscat/qscat_Ku2011_tech_report.pdf.

Richter, J. H., F. Sassi, and R. R. Garcia, 2010: Toward a physically based gravity wave source parameterization in a general circulation model. *J. Atmos. Sci.*, **67**, 136–156, https://doi.org/10.1175/2009JAS3112.1.

Rienecker, M. M., and Coauthors, 2011: MERRA: NASA's Modern-Era Retrospective Analysis for Research and Applications. *J. Climate*, **24**, 3624–3648, https://doi.org/10.1175/JCLI-D-11-00015.1.

Risien, C. M., and D. B. Chelton, 2008: A global climatology of surface wind and wind stress fields from eight years of QuikSCAT Scatterometer data. *J. Phys. Oceanogr.*, **38**, 2379–2413, https://doi.org/10.1175/2008JPO3881.1.

Rodwell, M. J., and T. N. Palmer, 2007: Using numerical weather prediction to assess climate models. *Quart. J. Roy. Meteor. Soc.*, **133**, 129–146, https://doi.org/10.1002/qj.23.

Sandu, I., P. Bechtold, A. Beljaars, A. Bozzo, F. Pithan, T. G. Shepherd, and A. Zadra, 2016: Impacts of parameterized orographic drag on the Northern Hemisphere winter circulation. *J. Adv. Model. Earth Syst.*, **8**, 196–211, https://doi.org/10.1002/2015MS000564.

Sardeshmukh, P. D., and B. J. Hoskins, 1984: Spatial smoothing on the sphere. *Mon. Wea. Rev.*, **112**, 2524–2529, https://doi.org/10.1175/1520-0493(1984)112<2524:SSOTS>2.0.CO;2.

Simpson, I. R., T. A. Shaw, and R. Seager, 2014: A diagnosis of the seasonally and longitudinally varying midlatitude circulation response to global warming. *J. Atmos. Sci.*, **71**, 2489–2515, https://doi.org/10.1175/JAS-D-13-0325.1.

Smith, S. D., 1988: Coefficients for sea surface wind stress, heat flux and wind profiles as a function of wind speed and temperature. *J. Geophys. Res.*, **93**, 15 467–15 474, https://doi.org/10.1029/JC093iC12p15467.

Svensson, G., and A. A. M. Holtslag, 2009: Analysis of model results for the turning of the wind and related momentum fluxes in the stable boundary layer. *Bound.-Layer Meteor.*, **132**, 261–277, https://doi.org/10.1007/s10546-009-9395-1.

Tokinaga, J., and S.-P. Xie, 2011: Wave- and anemometer-based sea surface wind (WASWind) for climate change analysis. *J. Climate*, **24**, 267–284, https://doi.org/10.1175/2010JCLI3789.1.

Trenberth, K. E., 1997: Using atmospheric budgets as a constraint on surface fluxes. *J. Climate*, **10**, 2796–2809, https://doi.org/10.1175/1520-0442(1997)010<2796:UABAAC>2.0.CO;2.

——, W. G. Large, and J. G. Olson, 1989: The effective drag coefficient for evaluating wind stress over the oceans. *J. Climate*, **2**,

1507–1516, https://doi.org/10.1175/1520-0442(1989)002<1507:TEDCFE>2.0.CO;2.

——, J. C. Berry, and L. E. Buja, 1993: Vertical interpolation and truncation of model-coordinate data. NCAR Tech. Note NCAR/TN-396+STR, 60 pp., https://opensky.ucar.edu/islandora/object/technotes%3A168.

——, J. T. Fasullo, and J. Mackaro, 2011: Atmospheric moisture transports from ocean to land and global energy flows in reanalyses. *J. Climate*, **24**, 4907–4924, https://doi.org/10.1175/2011JCLI4171.1.

van Neikerk, A., J. F. Scinocca, and T. G. Shepherd, 2017: The modulation of stationary waves, and their response to climate change, by parameterized orographic drag. *J. Climate*, **74**, 2557–2574, https://doi.org/10.1175/JAS-D-17-0085.1.

Wallace, J. M., S. Tibaldi, and A. J. Simmons, 1983: Reduction of systematic forecast errors in the ECMWF model through the introduction of an envelope orography. *Quart. J. Roy. Meteor. Soc.*, **109**, 683–717, https://doi.org/10.1002/qj.49710946202.

Wentz, F. J., and D. K. Smith, 1999: A model function for the ocean-normalized radar cross section at 14 GHz derived from NSCAT observations. *J. Geophys. Res.*, **104**, 11 499–11 514, https://doi.org/10.1029/98JC02148.

Yelland, M. J., B. I. Moat, P. K. Taylor, R. W. Pascal, J. Hutchings, and V. C. Cornell, 1998: Wind stress measurements from the open ocean corrected for airflow distortion by the ship. *J. Phys. Oceanogr.*, **28**, 1511–1526, https://doi.org/10.1175/1520-0485(1998)028<1511:WSMFTO>2.0.CO;2.

Zadra, A., 2015: WGNE drag project: An inter-model comparison of surface stresses. Environment Canada Tech. Rep. 1, 36 pp., http://collaboration.cmc.ec.gc.ca/science/rpn/drag_project/documents/wgne_drag_project_report01.pdf.

Zeng, X., Q. Zhang, D. Johnson, and W.-K. Tao, 2002: Parameterization of wind gustiness for the computation of ocean surface fluxes at different spatial scales. *Mon. Wea. Rev.*, **130**, 2125–2133, https://doi.org/10.1175/1520-0493(2002)130<2125:POWGFT>2.0.CO;2.

Zhang, G. J., and H.-R. Cho, 1991: Parameterization of the vertical transport of momentum by cumulus clouds. Part II: Application. *J. Atmos. Sci.*, **48**, 2448–2457, https://doi.org/10.1175/1520-0469(1991)048<2448:POTVTO>2.0.CO;2.